



UNIVERSITY OF LEEDS

This is a repository copy of *Discrete element modelling of the in-plane and out-of-plane behaviour of dry-joint masonry wall constructions*.

White Rose Research Online URL for this paper:  
<http://eprints.whiterose.ac.uk/144603/>

Version: Accepted Version

---

**Article:**

Bui, TT, Limam, A, Sarhosis, V [orcid.org/0000-0002-8604-8659](https://orcid.org/0000-0002-8604-8659) et al. (1 more author)  
(2017) Discrete element modelling of the in-plane and out-of-plane behaviour of dry-joint masonry wall constructions. *Engineering Structures*, 136. pp. 277-294. ISSN 0141-0296

<https://doi.org/10.1016/j.engstruct.2017.01.020>

---

© 2017 Elsevier Ltd. This manuscript version is made available under the CC-BY-NC-ND 4.0 license <http://creativecommons.org/licenses/by-nc-nd/4.0/>.

**Reuse**

This article is distributed under the terms of the Creative Commons Attribution-NonCommercial-NoDerivs (CC BY-NC-ND) licence. This licence only allows you to download this work and share it with others as long as you credit the authors, but you can't change the article in any way or use it commercially. More information and the full terms of the licence here: <https://creativecommons.org/licenses/>

**Takedown**

If you consider content in White Rose Research Online to be in breach of UK law, please notify us by emailing [eprints@whiterose.ac.uk](mailto:eprints@whiterose.ac.uk) including the URL of the record and the reason for the withdrawal request.



[eprints@whiterose.ac.uk](mailto:eprints@whiterose.ac.uk)  
<https://eprints.whiterose.ac.uk/>

# **Discrete element modelling of the in-plane and out-of-plane behaviour of dry-joint masonry wall constructions**

T. T. BUI<sup>1</sup>, A. LIMAM<sup>2</sup>, V. SARHOSIS<sup>3</sup>, M. HJIAJ<sup>4</sup>

<sup>1</sup>Université de Lyon, INSA Lyon, SMS-ID, France : [tan-trung.bui@insa-lyon.fr](mailto:tan-trung.bui@insa-lyon.fr),

<sup>2</sup>Université de Lyon, France : [ali.limam@insa-lyon.fr](mailto:ali.limam@insa-lyon.fr)

<sup>3</sup>School of Civil Engineering and Geosciences, Newcastle University, Newcastle, UK,  
[vasilis.sarhosis@newcastle.ac.uk](mailto:vasilis.sarhosis@newcastle.ac.uk)

<sup>4</sup>Université Européenne de Bretagne – INSA de Rennes, LGCGM/ Structural Engineering Research Group,  
France : [mohammed.hjjaj@insa-rennes.fr](mailto:mohammed.hjjaj@insa-rennes.fr)

## **Abstract**

This paper aims to improve knowledge on the suitability of the discrete element method (DEM) to simulate the in-plane and out-of-plane behaviour of different in-configuration structural masonry walls constructed with dry joints. The study compares the results obtained from laboratory tests against those predicted using the three-dimensional distinct element 3DEC software. Significant features of the structural behaviour shown by the walls are discussed and conclusions on their ultimate capacity and failure mechanisms are addressed. A key feature of the DEM is the important role that brick discontinuities, i.e. joints, play in the mechanics of masonry. Within DEM, the bricks were modelled as continuum rigid elements while the joints were modelled by line interface elements represented by the Mohr-Coulomb law. The analysis of the results showed that the model developed is capable of representing the crack development and load carrying capacity of masonry structures constructed with dry joints with sufficient accuracy. Moreover, a collection of experimentally verified material parameters is provided to be used by other researchers and engineers and to develop a reliable model to solve engineering challenges worldwide.

Keywords: masonry; discrete element method; dry joints; out-of-plane loading; earthquake.

## 1. Introduction

Masonry is a common and traditional form of construction that has been used for centuries around the world. Some of the most important cultural and historical monuments (such as the Parthenon, the pyramids, the Colosseum and the Segovia aqueduct) were constructed using masonry. Many of these masonry structures were constructed without mortar (dry joints). Examples include the famous Aqueduct in Segovia, Spain, and the Pont du Gard in France, the temples of the ancient Khmer Empire in Cambodia, the City of Great Zimbabwe in Africa and certain Medieval monasteries built in the south of Europe. **Figure 1** shows typical old masonry structures constructed with dry joints. Moreover, a number of historical and old constructions, originally built with mortar joints, have experienced significant loss of mortar due to chemical, physical and mechanical degradation. Examples include masonry arch bridges and other civil engineering structures currently in use such as tunnel linings and earth-retaining walls. In these cases, the masonry-unit to mortar-joint bond is disrupted by environmental erosion (e.g. weathering and/or the action of water leeching through the mortar joints over a prolonged period). Due to the partial or total disappearance of mortar, the behaviour of these constructions becomes similar to those made of dry-joint masonry. Research in the area of masonry constructions made of dry joints is therefore essential to understand their behaviour when exposed to external loading and assess their design levels in order to inform repair and/or strengthening decisions. The possibility of performing destructive tests on historical/old constructions, either in situ or by removing samples large enough to be representative, is usually impossible (Macchi 1992). In addition, full-scale experimental tests are prohibitively expensive. Therefore, it is fundamentally important to have available computational tools to predict the in-service and near-collapse behaviour of such complex structures with sufficient reliability. Once such a tool has been established, a range of complex problems and scenarios can be investigated.



(a) Ancient Andean stoneworks in Machu Piccu, Peru



(b) Classical Inca architectural style of polished dry-stone walls of regular shape in Machu Piccu, Peru



**Figure 1.** Masonry structures constructed with dry masonry joints

So far, research on numerical modelling of structural masonry has mostly investigated the characterization of mortared-joint masonry. A broad range of numerical methods is available today, ranging from the classical plastic solution methods (Heyman, 1998) to the most advanced non-linear computational formulations (e.g. finite element and discrete element methods [DEM] of analysis). According to Lourenço (1996), the strategies available for the numerical modelling of masonry structures would fall within one of two categories: a) micro-scale and b) macro-scale modelling. In macro-scale modelling, the masonry units and mortar joints smeared out into an averaged continuum. There are no distinctions between the units, the mortar and their interfaces. This model can be applied when the dimensions of a structure are large enough, compared to the constituent parts, so that a description involving average stresses and strains becomes acceptable (Chaimoon & Attard 2007). Considerable computational time is saved by applying this method. However, unconditionally accurate results and the fine details of the behaviour cannot be captured by this type of approach. On the other hand, micro-scale modelling splits into the following two approaches: a) simplified micro-modelling and b) detailed micro-modelling. In the simplified micro-modelling approach, expanded units are modelled as continuous elements while the behaviour of the mortar joints and unit–mortar interface is lumped in discontinuous elements. In the detailed micro-modelling approach, both the masonry units and the mortar are discretized and modelled with continuous elements while the unit–mortar interface is represented by discontinuous elements accounting for potential crack or slip planes. Detailed micro-modelling is probably the most accurate tool available today to simulate the real behaviour of masonry given that the elastic and inelastic properties of both the units and the mortar can be realistically taken into account. In this method, a suitable constitutive law is introduced to reproduce not only the behaviour of the masonry units and mortar, but also their interaction. However, any analysis within this level of refinement requires substantial computational power. Therefore, this method is used mainly to simulate tests on small specimens to accurately determine the stress distribution in the masonry materials. The drawback of the substantial computational power required by detailed micro-modelling is partially overcome by the simplified micro-modelling strategy. In this case, each joint, consisting of mortar and the two unit–mortar interfaces, is lumped into an “average” interface while the units expand in size in order to keep the geometry unchanged. Within this approach, it is possible to consider masonry as a set of elastic blocks bonded together by potential fracture slip lines at the joints. The main methods available for modelling masonry structures using the simplified micro-modelling approach include: a) the discontinuous finite element method and b) the DEM. The material discontinuity introduced by the joints in dry-joint masonry constructions makes the use of interface elements an appropriate option to model such structures.

When modelling masonry using the discontinuous finite element method, discontinuities are introduced using interface elements, for which the constitutive model is in direct relation with the stress vector and the relative displacement vector along the interface (Oliveira 2003). Therefore, for an accurate simulation of masonry behaviour, it is essential to obtain a constitutive model for the interface elements which is able to

capture the behaviour of masonry realistically and to simulate all the failure mechanisms. Page (1978) first introduced masonry as a two-phase material composed of bricks and a zero-thickness interface. Bricks were represented as a linear elastic material and interfaces as inelastic, obeying the Mohr-Coulomb failure criterion. Lourenço (1996) subsequently introduced a compressive cap to the failure surface in Page's model, allowing all possible failure modes. Although a micro-scale model needs more computational time, it can let many salient behaviour features emerge, thus providing a better understanding of the phenomenon involved and predicting the masonry walls' performance. More recently, Casapulla et al. (2014) developed two macro- and micro-block models and solution procedures within three-dimensional limit analysis. They highlighted the predominant role that frictional resistance plays in the masonry buildings without a box-type action and the need to further understand the behaviour of dry-joint masonry. Their models were based on a concave contact formulation in which contact points are located at the corners of interfaces, allowing failure modes involving opening and sliding to be simulated. An iterative solution procedure was used to solve the non-associative friction problem, with second-order cone programming to allow the conic yield function to be solved directly. However, in such models, the dynamic friction was not taken into account and could potentially result in an overestimation of the out-of-plane capacity of the system represented.

The DEM falls within the simplified micro-modelling approach and involves modelling the materials as an assemblage of distinct blocks or particles interacting along their boundaries. In this way, the heterogeneous nature of masonry joints is explicitly described. According to its developers, Cundall and Hart (1992), the term "discrete" only applies to a computational model if: a) it allows finite displacements and rotations of discrete bodies and b) new contacts between the blocks or particles are automatically recognized and updated as the calculation progresses. The formulation of the method was initially proposed for the study of jointed rock, modelled as an assemblage of rigid blocks. Later the approach was extended to other fields of engineering requiring a detailed study of the contact between blocks or particles such as soil and other granular materials (Ghaboussi and Barbosa 1990). Recently, the approach was successfully applied to model the in-plane mechanical behaviour of rammed-earth materials (Bui et al. 2016) and masonry structures containing low-bond-strength mortar joints in which the collapse modes were typically governed by mechanisms in which the deformability of the blocks plays little or no role (Sarhosis & Sheng 2014; Sarhosis et al. 2014; Giamoundo et al. 2014; Lemos 1995; Sarhosis 2016).

This paper aims to improve the knowledge of the in-plane and out-of-plane mechanical behaviour of different configurations of dry masonry walls, and to challenge an existing sophisticated non-linear interface modelling tool based on the DEM of analysis. The assessment consisted of a comparison of the results from full-scale laboratory tests with the behaviour predicted using the three-dimensional distinct element (DE) modelling software, 3DEC. Significant features of the structural behaviour shown by the walls are discussed and conclusions on their ultimate capacity and observed failure mechanisms are addressed. Moreover, a collection of experimentally verified material parameters that could reliably be used by other researchers and engineers to develop similar computational models are presented.

## 2. Overview of the discrete element method

The discrete element method (DEM) falls within the general classification of discontinuous analysis techniques. The method was developed by Cundall in the early 1960s for numerical research into the sliding of earth and rock masses. It is now presented in the commercial codes UDEC (Universal Distinct Element Code) and 3DEC software for two- and three-dimensional simulations, respectively. Over the last three decades, the software has been used for a range of applications, including masonry wall panels (Sarhosis & Sheng 2014; Sarhosis et al. 2015; Bui et al. 2010; Bui et al. 2014), retaining walls (Claxton et al. 2006), masonry-infilled steel frames with openings (Mohebkhah et al. 2008; Sarhosis et al. 2014a), stone masonry arches and aqueducts (Roberti 2001; Roberti and Calvetti 1998; Lemos 2004; Tóth et al. 2009; Sarhosis et al. 2014b) and column-architrave structures under seismic action (Papantonopoulos et al. 2002; Psycharis et al. 2003; Stefanou 2011).

In 3DEC, masonry units are represented as an assembly of rigid or deformable blocks, and blocks are represented as convex polyhedra in 3D with each face being a planar convex polygon with rectilinear edges. Rigid blocks do not change their geometry under applied loading. Deformable blocks are discretized into triangular zones of uniform stress characteristics. These zones are continuous elements as they occur in the finite element method (FEM). However, unlike FEM, in the DEM a compatible finite element mesh between the blocks and the joints is not required. A zero-thickness interface between the blocks represents the mortar joints, the contact between blocks is not based on joint elements, as occurs in the discontinuous finite element models. Instead, the contact is represented by a set of point contacts with no attempt to obtain a continuous stress distribution through the contact surface. The assignment of contacts allows the interface's constitutive relations to be defined in terms of the stresses and relative displacements across the joint.

The model definition in 3DEC corresponds to the domain discretization by a series of blocks. Blocks can take any arbitrary geometry and may be different from each other in size and shape. Individual blocks can be rigid or deformable. Rigid blocks are used when the behaviour of the system is dominated by the joints. Alternatively, the blocks are modelled as deformable and the complexity of the deformation of the blocks depends on the number of zone elements into which they are divided. Zones obey the constitutive model assigned to them; in this way, the strain is estimated for each separate block. In 3DEC, the deformable block zones can be assumed to be linear elastic or non-linear according to the Mohr-Coulomb criterion (ITASCA, 2004). The material parameters for the linear, isotropic, elastic model are the Poisson ratio, elastic modulus (E) and shear modulus (G).

In 3DEC, a zero-thickness interface between adjacent blocks characterizes the joints. At these interfaces, the blocks are connected to each other by sets of point contacts. These contact points are located at the outside perimeter of the blocks and created at the edges or corners of the blocks and zones. For each contact

point, there are two spring connections (**Figure 2**), as described in Cundall and Hart (1992). These can transfer either a normal force or a shear force from one block to another.

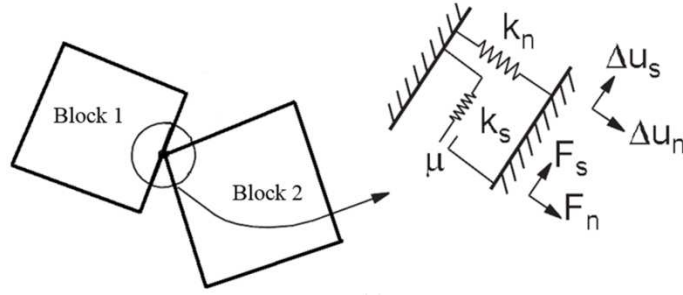


**Figure 2.** Mechanical representation of the contact between blocks

The interfaces between blocks are simulated by the Mohr-Coulomb interface model with a tension cut-off, which considers both shear and tensile failure. The joint interface dilation is also included. In the elastic range, the behaviour is governed by normal and shear stiffness of the interface  $k_n$ , and  $k_s$ :

or

$$\Delta\tau_s = k_s\Delta u_s \quad (1)$$

$$\Delta\sigma_n = k_n\Delta u_n \quad (2)$$

where  $\sigma_n$  is the normal stress,  $u_n$  is the normal displacement,  $\tau_s$  is the shear stress and  $u_s$  is the shear displacement. The maximum shear stress allowed is given by:

$$\tau_{max} = c + \sigma_{n(max)} \cdot \tan \phi \quad (3)$$

where  $c$  and  $\phi$  are the interface cohesion and friction angle, respectively. After the peak strength has been reached, shear strength drops until a residual strength  $\tau_{res}$  is obtained (**Figure 3a**):

$$\tau_{res} = \sigma_{n(max)} \cdot \tan \phi \quad (4)$$

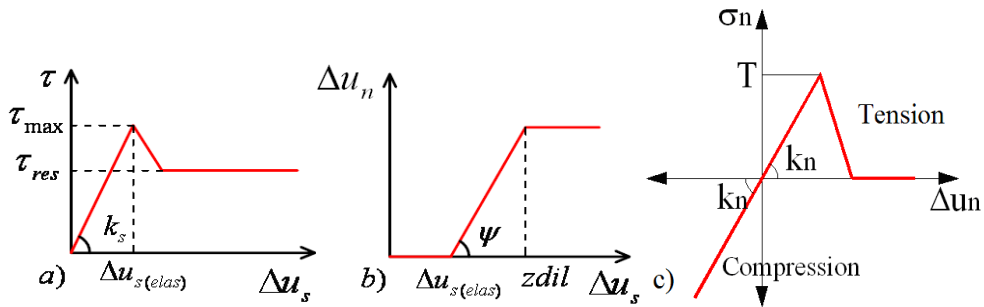


**Figure 3.** Mechanical interface behaviour: a) Mohr-Coulomb slip model; b) bilinear dilatant model; c) behaviour under uniaxial loading.

As indicated in **Figure 3b**, the zero-thickness interfaces begin to dilate when mortar fails in shear, at shear displacement  $\Delta u_s$  as a function of the dilatation:

$$\Delta u_{n,dilatation} = \Delta u_s \tan \psi \quad (5)$$

where  $\psi$  is the dilatancy angle and  $\Delta u_n$  the normal displacement. The normal stress is corrected to take into account the effect of dilatation:

$$\sigma_{n,total} = \sigma_{n,elastic} + \sigma_{n,dilatation} = k_n \cdot \Delta u_n + k_n \cdot \Delta u_{n,dilatation} = k_n \cdot \Delta u_n + k_n \cdot \Delta u_s \tan \psi \quad (6)$$

When dilatation is presented, the shear displacement is in the plastic phase ( $\Delta u_s > \Delta u_{s,elas}$ , **Figure 3a**). The normal displacement is assumed to be linear until  $z_{dil}$  (**Figure 3b**). Dilatation increases if the shear displacement increment runs in the same direction as the total shear displacement and decreases if the shear increment runs in the opposite direction. The extension occurs until the limiting shear displacement ( $z_{dil}$ ) is reached. The interface behaviour under uniaxial loads is shown in **Figure 3c**, where  $T$  is the interface tensile strength. Before the tensile failure ( $\sigma_n < T$ ), an elastic behaviour is assumed.

3DEC is based on an explicit time integration method that solves the equations of block system motion by an explicit finite difference method. A solution scheme based on the equations of motion was demonstrated to be better suited to indicate potential failure modes of discontinuous systems than schemes which disregard velocities and inertial forces. At each time step, the law of motion and the constitutive equations are applied. For both rigid and deformable blocks, sub-contact force–displacement relations are prescribed. The integration of the law of motion provides the new block positions and therefore the contact displacement increments (or velocities). The sub-contact force–displacement law is then used to obtain the new sub-contact forces, which will be applied to the blocks in the next time step.

Mechanical damping is used in the distinct element method to solve two general classes of problems: static (non-inertial) solutions and dynamic solutions. For static analysis, the approach is conceptually similar to dynamic relaxation, proposed by Otter et al. (1966). Two alternative forms of velocity-proportional damping are available in 3DEC: a) adaptive global damping and b) local damping. Adaptive global damping is used to adjust the damping constant automatically. Viscous damping forces are used, but with the viscosity constant continuously adjusted in such a way that the power absorbed by damping is a constant proportion of the rate of change of kinetic energy in the system. 3DEC provides another form of damping, in which the damping force on a node is proportional to the magnitude of the unbalanced force. For this scheme, referred to as local damping, the direction of the damping force is such that energy is always dissipated. From ITASCA (2004), it is recommended to use local damping for static analyses. This is generally appropriate for static analysis. In addition, local damping is more suitable to minimize oscillations that may arise when abrupt failure occurs in the model. In this study, local damping with the default damping value of 0.8 used.

### **3. In-plane behaviour of masonry walls constructed with dry joints**

#### **3.1 Masonry wall subjected to vertical in-plane load**

The first case study investigates the mechanical behaviour of a brick masonry wall subjected to vertical in-plane load to represent ground movement as differential settlement. Three full-scale single-leaf brickwork masonry wall panels were tested in the laboratory (CL1–CL3). The wall panels were 1,575 mm × 1,000 mm ×

220 mm (span × height × breadth) and had 20 courses of stretcher-bonded brickwork. The typical arrangement of the CL1 test panel is shown in **Figure 4**.

All the test panels were constructed with standard size 50 × 105 × 220 mm (height × span × breadth) bricks. The bricks had an average compressive strength of 35 N/mm<sup>2</sup> and a unit weight equal to 2,200 kg/m<sup>3</sup>. All wall panels were constructed with dry joints (i.e. no mortar joints). Therefore, shear between the masonry bricks was purely due to friction. The angle of friction between the faces of the bricks was calculated experimentally and found to be equal to 38°.

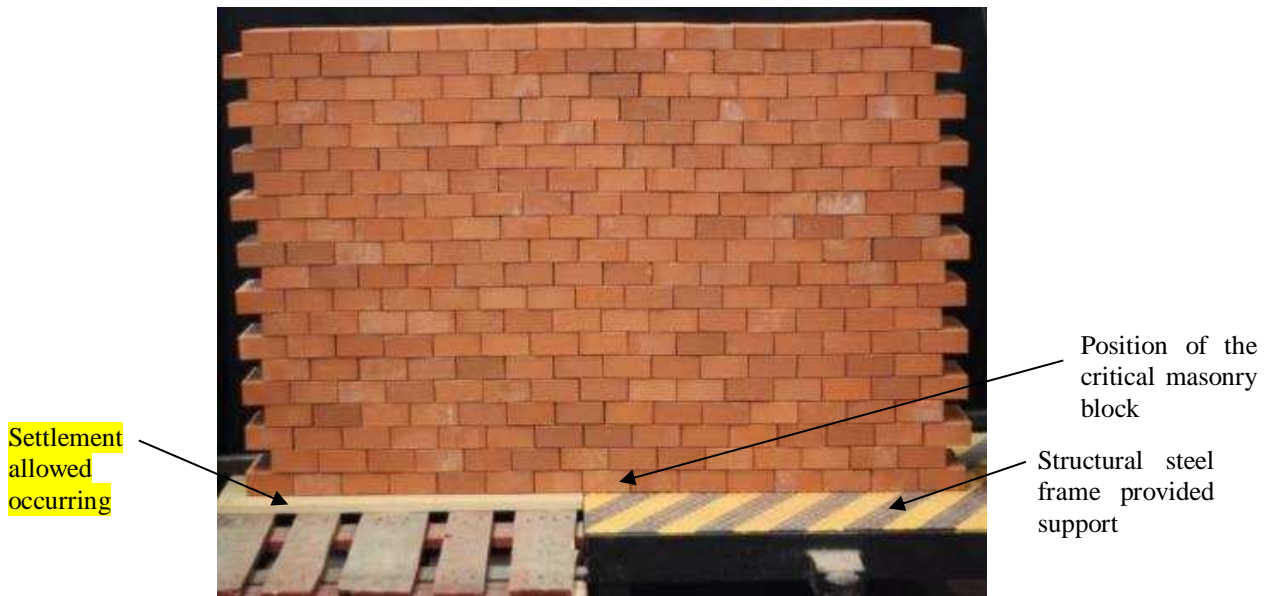


**Figure 4.** Configuration of the test CL1

??

Each wall panel was tested under gravity load. A vertical settlement was assigned artificially using a hydraulic ram (e.g. controlled constant velocity in the downward direction) at the left-hand side of the wall. Settlement was applied to each panel up to a height of 140 mm with a velocity equal to 2 mm/s. A structural steel frame provided the support at the right-hand side of the wall (**Figure 4**). Settlement was applied to each wall incrementally until the panel could no longer carry its load. For each artificial settlement increment, vertical deflections were measured using dial gauges located at the middle of the left-hand side of the wall (settlement side). The surfaces of the panels were inspected visually for signs of opening at each stage of the experiment. The experimental test results are summarized in **Figure 5**.

In **Figure 5**, the observed failure mode varied depending on the boundary condition and brick arrangements. The difference in the boundary conditions for the wall panels (CL1, CL2 and CL3) was due to the position of a critical masonry block, which was sometimes positioned at the location where settlement allowed occurring (left side) and others were positioned above the structural steel frame (right side). For the CL1 test, the masonry block laid entirely above the structural steel frame (right-hand side) (ref. Figure 4). For the CL2 to CL3 experimental tests, the block was positioned one-quarter of its length towards the settlement area (left side). While testing the CL3 panel, the block rotated significantly, which influenced the failure pattern

(Figure 5). Figure 5 shows that the experimental failure mode was characterized by two major cracks. The first crack appeared at the centre of the wall and resulted from bending. The second crack appeared at the left-hand side and at the bottom of the panel in the location where settlement took place, resulting in the formation of a brick-stacked pyramid.

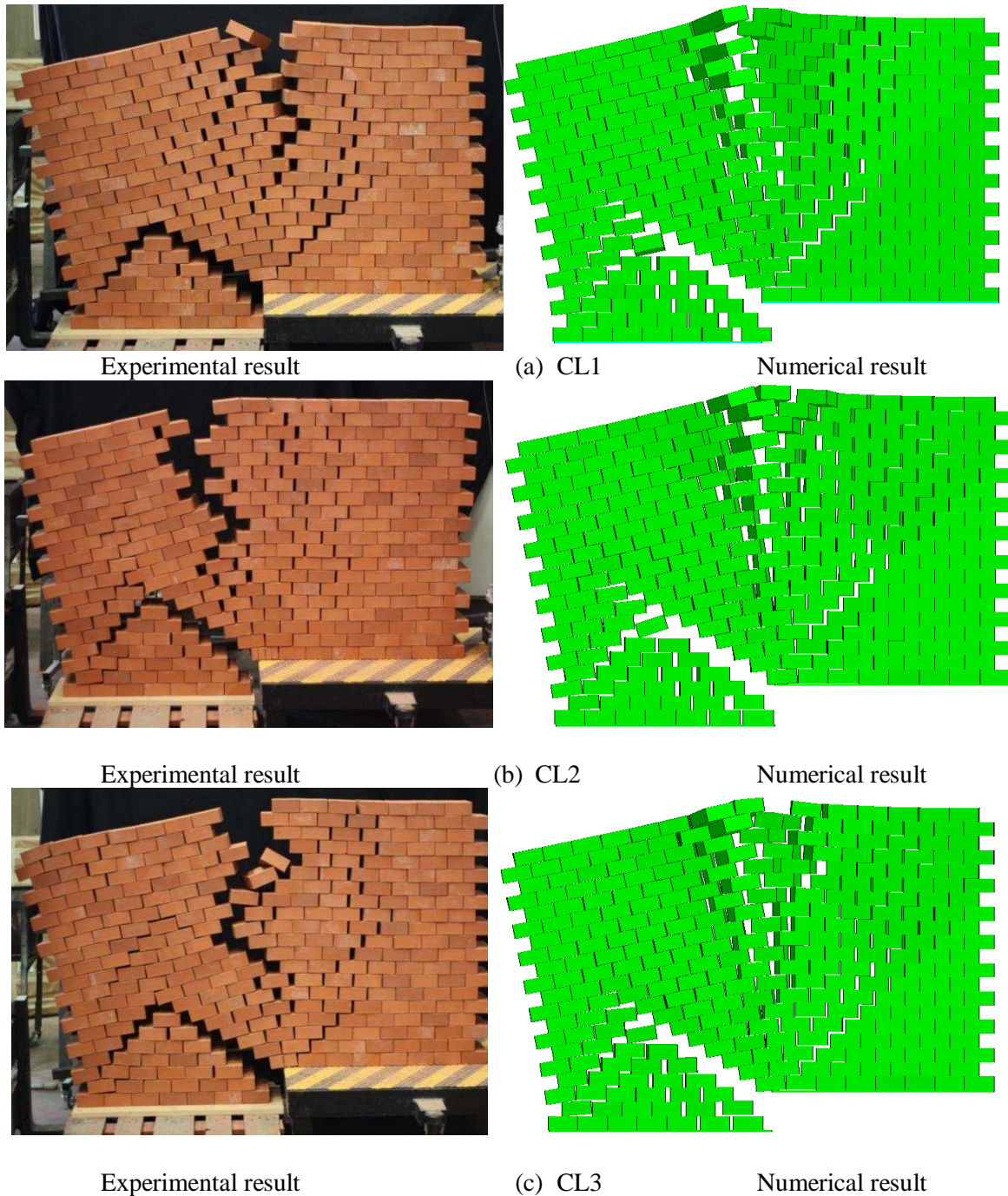


**Figure 5.** Comparison of experimental and numerical failure modes of the masonry wall panels for the different boundary conditions studied

Geometrical models representing the brickwork masonry wall panels tested in the laboratory were accurately modelled using 3DEC discrete element software. Each brick of the panel is represented by a rigid block separated by zero-thickness interfaces at each mortar bed and perpend joint. Material properties were

selected such that the bricks would remain intact at all stages of loading and the predominant failure mode would slip along the zero-thickness interface. The block parameters required by 3DEC to represent the behaviour of the bricks are the unit weight ( $d$ ), the elastic modulus ( $E$ ), the shear modulus ( $G$ ) and the Poisson ratio ( $\nu$ ). Mortar joints were represented by interfaces modelled using 3DEC's elastic-perfectly plastic coulomb slip-joint area contact. The normal ( $k_n$ ) and shear ( $k_s$ ) stiffness of the zero-thickness interface were calculated based on equations 7 and 8 and obtained from Lourenço et al. (2005).

$$k_n = \frac{1}{\left(\frac{1}{E_m} - \frac{1}{E_b}\right) \times h_b} = \frac{E_b \cdot E_m}{(E_b - E_m) \times h_b} \quad (7)$$

and

$$k_s = \frac{k_n}{2(1 + \nu)} \quad (8)$$

where  $E_m$  is the Young modulus of the wall in  $\text{N/mm}^2$ ,  $E_b$  is the Young modulus of the masonry block in  $\text{N/mm}^2$ ,  $h_b$  is the height of the masonry block and  $\nu$  is the Poisson ratio. The Young modulus of masonry block  $E_b$  was taken equal to 9,700 MPa and the height of block ( $h_b$ ) was taken equal to 50 mm. Also, the Poisson ratio was assumed to be 0.2 while the Young modulus of the wall  $E_m$  was assumed to be equal to 1% of the Young modulus of the block ( $E_b$ ), giving a value of 97 MPa. By substituting equations (7) and (8), we obtained the normal stiffness value equal to  $1.96 \text{ N/mm}^3$  and the shear stiffness value equal to  $0.82 \text{ N/mm}^3$ . The friction angle was measured experimentally and found to be equal to  $38^\circ$ . Also, since we were modelling dry masonry joints, the interface cohesive, tensile strength and the dilatation angle were set to zero. Self-weight effects were also included in the model as gravitational load. First, the model was brought into a state of equilibrium under its own weight. Then a vertical constant downward velocity equal to 2 mm/s was applied to the bottom spreader plate of the wall until collapse. To check the validity of the numerical procedure, the experimental behaviour of the wall panel was compared to the behaviour predicted by the numerical model. However, the force-displacement diagram was not recorded during the experiment. Therefore, the computational and experimental results were compared qualitatively (i.e. comparing the failure modes). As illustrated in **Figure 5**, the DEM model was found to be capable of representing the experimental failure modes of the masonry wall panels with sufficient accuracy. To assess the suitability of the computational model to quantitatively predict the mechanical behaviour of masonry constructed with dry joints, we extended the study and simulated the experiments carried out by Lourenço (2005), as described in the next section of the paper.

### 3.2 Masonry wall subjected to combined shear and vertical pre-compression.

The second case study examines the in-plane behaviour of a masonry wall panel constructed with dry joints subjected to combined shear and axial pre-compression. A numerical model based on DEM was developed and the numerical results were compared with experimental results obtained from the literature (Lourenço 2005). All masonry wall panels were  $1,000 \text{ mm} \times 1,000 \text{ mm} \times 200 \text{ mm}$  (height  $\times$  span  $\times$  breadth) in size and constructed using  $100 \text{ mm} \times 200 \text{ mm} \times 200 \text{ mm}$  (height  $\times$  span  $\times$  breadth) blocks. All masonry

blocks were cut mechanically, leaving a smooth surface. An embedded concrete beam was placed at the top of the wall where vertical load was assigned at different pre-compression levels: 30 kN (SW30-1 and SW30-2), 100 kN (SW100-1 and SW100-2), 200 kN (SW200-1 and SW200-2) and 250 kN (SW250). Initially, a vertical compressive load was applied by means of a hydraulic actuator with a capacity of 1,000 kN, under force control at a rate of 1 kN/s, until the desirable load was totally applied to the wall. Subsequently, the hydraulic actuator was kept under force control, resulting in an applied constant vertical load. Consequently, the beam was allowed to move in the vertical and horizontal directions. Afterwards, the horizontal load was applied by imposing small increments of displacement. For this purpose, a hydraulic actuator was horizontally fixed and load was applied at the reinforced concrete beam. In the numerical model, the friction angle of the joint interface was set to  $32^\circ$  (Lourenço 2005), while the cohesive strength, tensile strength and angle of dilatancy of the zero-thickness interface were set to zero.

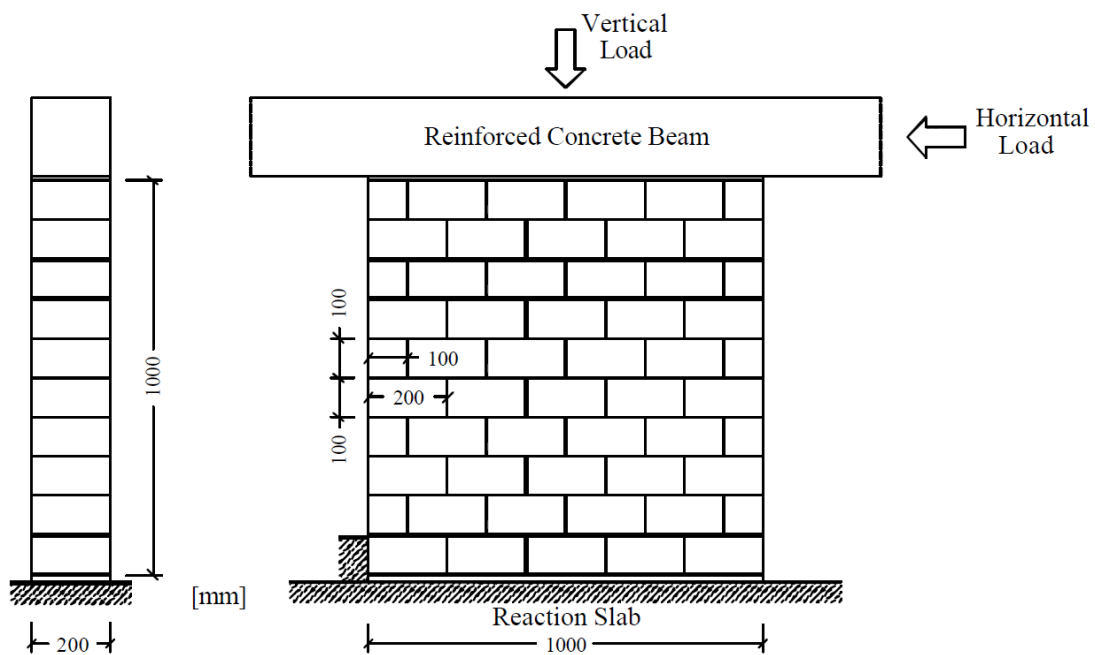


**Figure 6.** Adopted geometry for the dry masonry wall and applied loading (Lourenço 2005)

Reinforced concrete beam; Vertical load; Horizontal load, Reaction slab

Normal and shear stiffness of the zero-thickness interfaces calculated according to equations 7 and 8 as obtained from Lourenço et al. (2005). The  $E_b$  is the Young modulus of the masonry block taken as  $15,500 \text{ N/mm}^2$ , the height of the stone  $h_b$  taken as 100 mm and the Poisson ratio equal to 0.2. Table 1 shows the values of the Young modulus  $E_m$  for the different masonry walls under consideration here. In Table 1, the Young modulus increases as the vertical load increases, which means that the masonry made by assembling dry stone has a particular nonlinear elastic behaviour, with increased rigidity in the vertical compression.

**Table 1.** Summary of  $E_m$  and  $k_n$   $k_s$

Wall	$E_m$ [N/mm <sup>2</sup> ]	$k_n$ [N/mm <sup>3</sup> ]	$k_s$ [N/mm <sup>3</sup> ]
SW30	556	5.87	2.45
SW100	768	8.08	3.37

SW200	1057	11.40	4.73
SW250	1202	13.00	5.43

**Figure 7** compares the failure mode of the wall panel observed experimentally with the one predicted from the numerical model. The experimental results showed that there were three notable aspects of behaviour, namely: a) de-bonding of the top concrete beam, followed by b) diagonal stepped crack initiated from the top right-hand corner of the wall, with excessive load leading to c) crushing of the stone masonry units. **Figure 7** shows the failure mode predicted by the numerical model found to be similar to the failure mode obtained experimentally. However, the numerical model did not capture crushing the stone masonry units due to the linear elastic assumption of the masonry units adopted in numerical model.

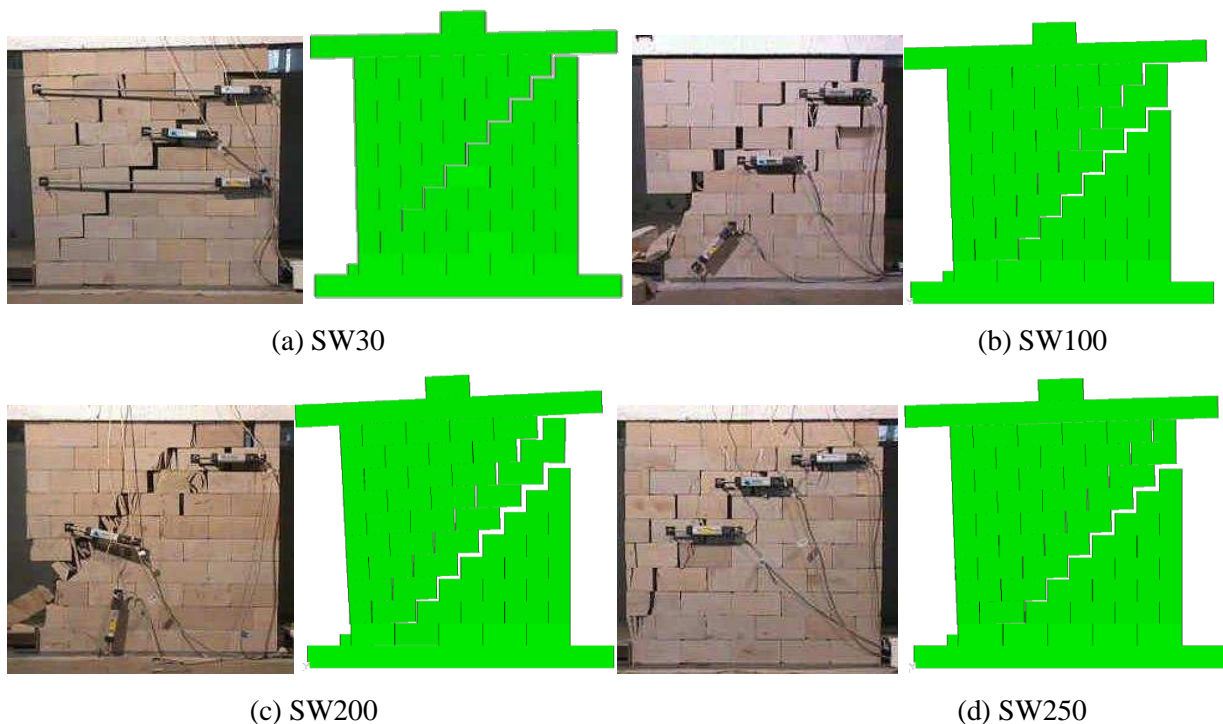
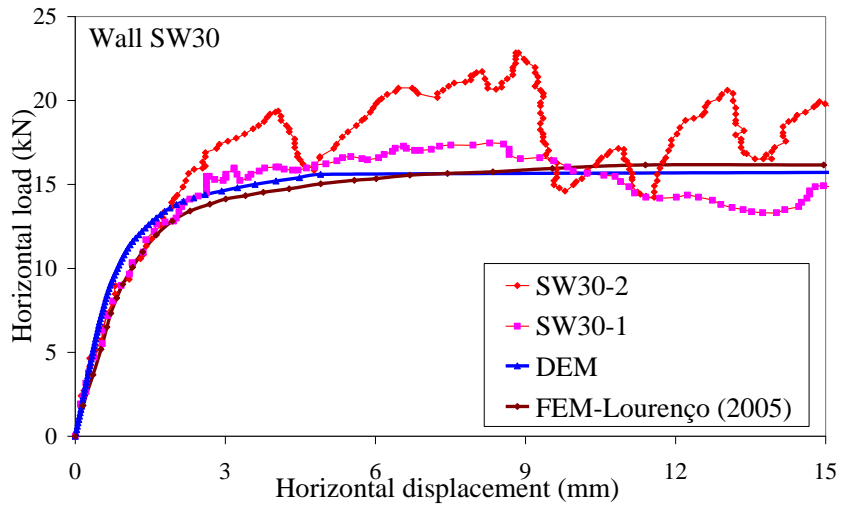
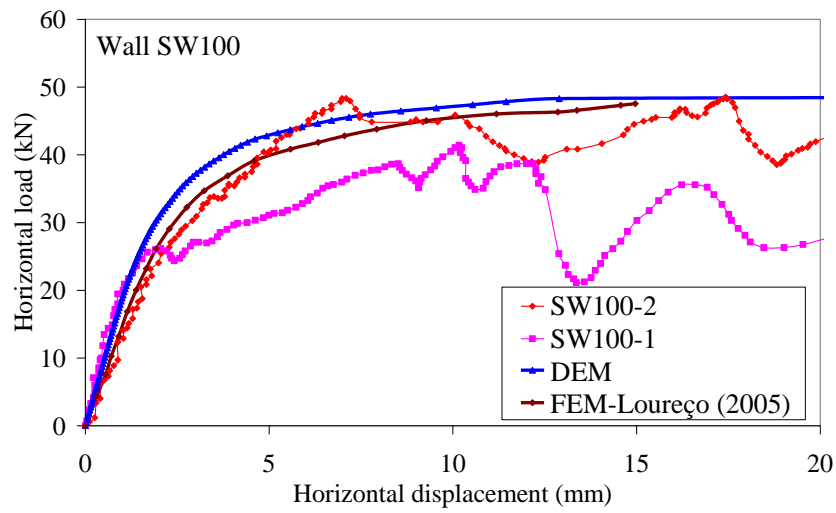


**Figure 7.** Failure modes for the wall specimens: experimental test (Lourenço 2005) vs numerical simulation by DEM

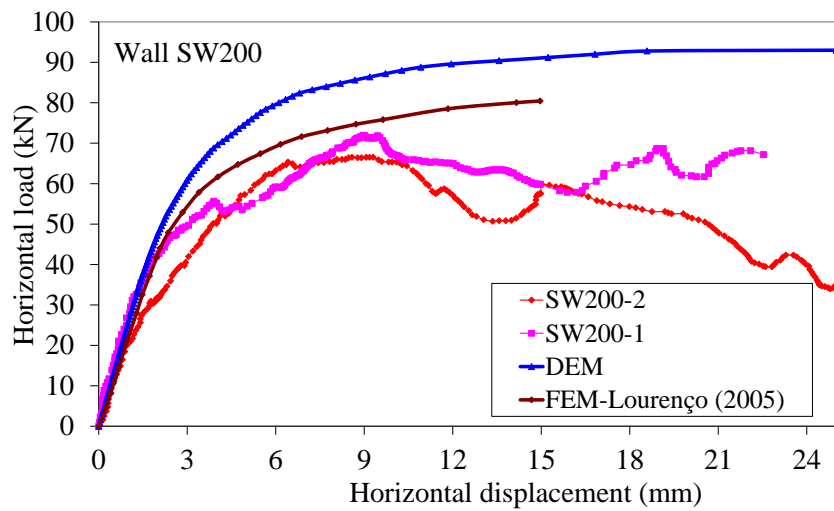
Comparisons of the experimental and the numerical (both FEM and DEM) load deflection curves of the masonry wall panels (SW30-1, SW30-2, SW100-1, SW100-2, SW200-1, SW200-2, SW250) are presented in **Figure 8**. For the wall panels SW30 and SW100, the experimental load versus the displacement relationship is very similar to that predicted by the DEM (**Figure 8a** & **Figure 8b**). Also, the predicted load–displacement relationship using the FEM model developed by Lourenço (2005) is similar to the relationship predicted by the DEM model. However, the load–displacement relationship predicted by the DEM model differs for the wall panels SW200 and SW250 because of the inability of the DEM model to capture the crack development at the masonry unit level.



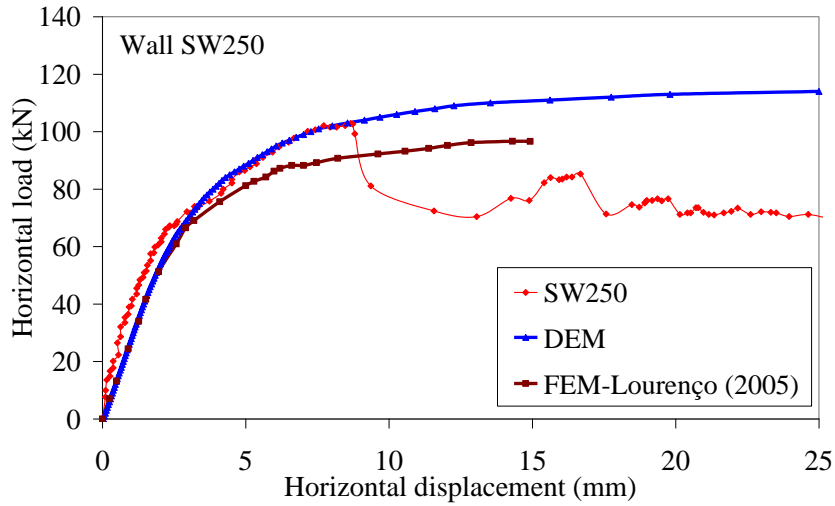
a) Wall SW30



b) Wall SW100



c) Wall SW200



d) Wall SW250

**Figure 8.** Load-deflection curve comparison: Experiments, DEM & FEM according to (Lourenço, 2005)

#### 4. Out-of-plane loading

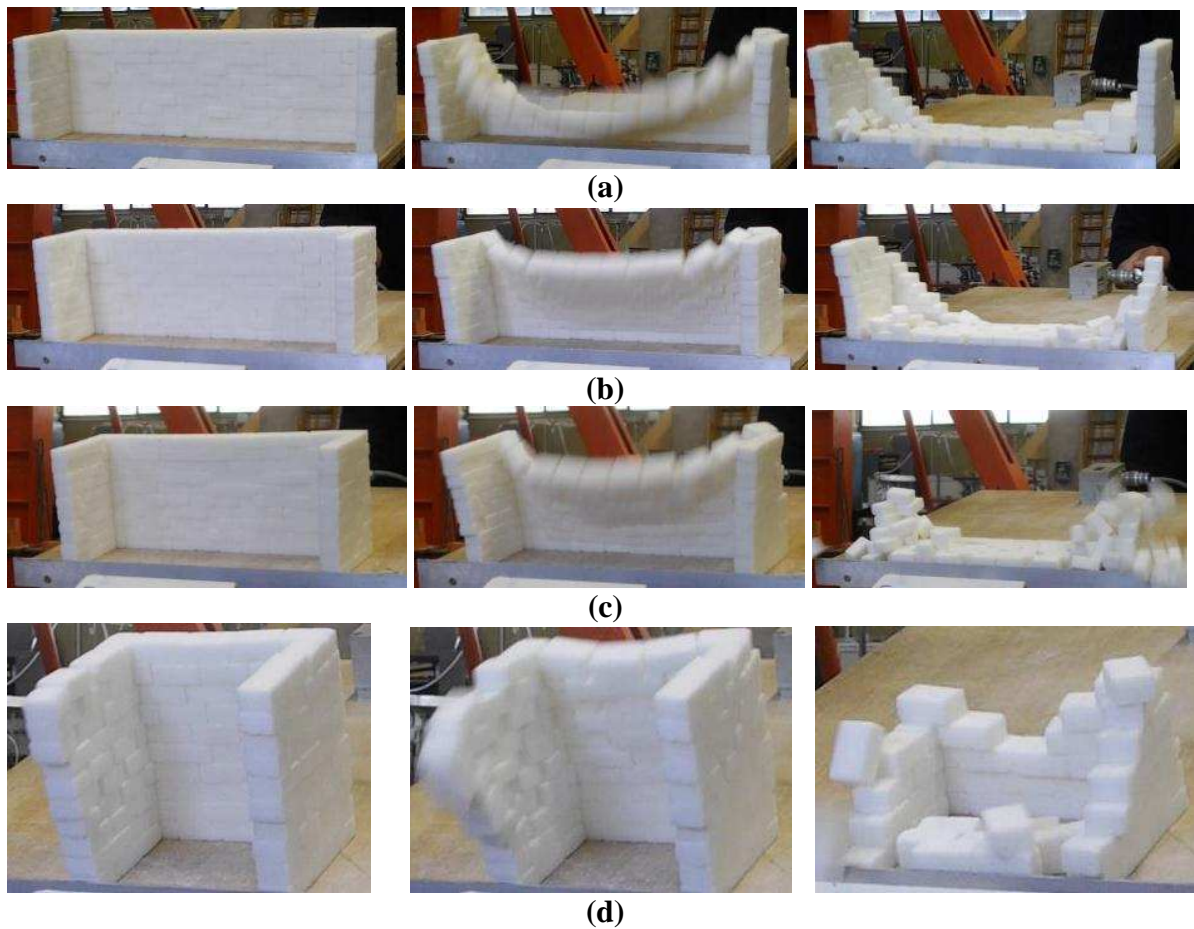
##### 4.1 Quasi-static loading - Scaled model 1/10

A scale model of a masonry wall connected with two perpendicular partition walls was tested in the laboratory. The walls constructed with masonry units made of sugar blocks and placed one on top of the other with no joint material (i.e. dry joints). Sugar blocks were 27 mm × 12 mm × 17 mm in size (length × height × thickness), 1/10 compared to actual masonry unit dimensions. The unit weight of the sugar blocks was 1,081 kg/m<sup>3</sup>, which is almost half of the unit weight of the original masonry units. The friction angle between the faces of the sugar blocks was measured experimentally and found to range from 28.5° to 32°. For the numerical model developed in this study, the input friction angle was equal to 30.4°, and the masonry units were modelled as rigid blocks. The dimensions of the central wall was 400 mm × 125 mm × 17 mm (length × height × thickness) and was connected with two partition walls 98 mm × 125 mm × 17 mm (length × height × thickness). Geometrical sensitivity studies were carried out to assess the influence of the length over the height (L/H) ratio of the wall. Four different geometries considered where the L/H was equal to: a) 3.2, b) 2.7, c) 2.3 and d) 1. For all the experimental tests, the dimensions of the two partition walls remained the same. The base of the structure was elevated using a tilting table, and for each of the small-scale experiments, the tilting angle (or the “critical angle”) at collapse was recorded. Analytically, the acceleration required to cause collapse of the wall was estimated by (Dejong, 2009):

$$a_{\text{critical}} = g * \sin (\varphi_{\text{cr}}) \quad (9)$$

where  $g$  is the gravitational acceleration and  $\varphi_{\text{cr}}$  is the critical tilting angle. **Figure 9** shows the failure modes of the wall panels observed in the experiment. As shown in **Figure 9**, the masonry walls failed in the out-of-plane direction due to bending. The images shown in **Figure 9** were taken just before the complete collapse (approximately 1 s before the collapse). During the experimental testing, the wall collapsed very quickly. A high-speed camera (24 frames/s) was used to extract these images. In **Figure 9**, for the same tilting angle, the

collapse due to bending is more evident for the cases where the L/H ratio is greater. For the cases with a small L/H ratio value, the bending effect is progressively inhibited, leaving the effects of torsional and mainly the sliding and shear effects that will interact and control the collapse. Geometrical models representing the brickwork masonry wall panels tested in the laboratory were created using the discrete element software 3DEC. Analysis of the results demonstrated that the DEM model developed is capable of accurately predicting the mode of failure and crack propagation (**Figure 9e** & **Figure 9f**). The results were also compared quantitatively. **Figure 10** compares the numerical with the experimental critical tilting angle in relation to the L/H ratio: although the trend of the graphs is similar, there is an offset of approximately 5 degrees in the predicted critical tilting angle because of the heterogeneous behaviour of the properties of the block interface. In the numerical model, an average friction angle of the interface was used.



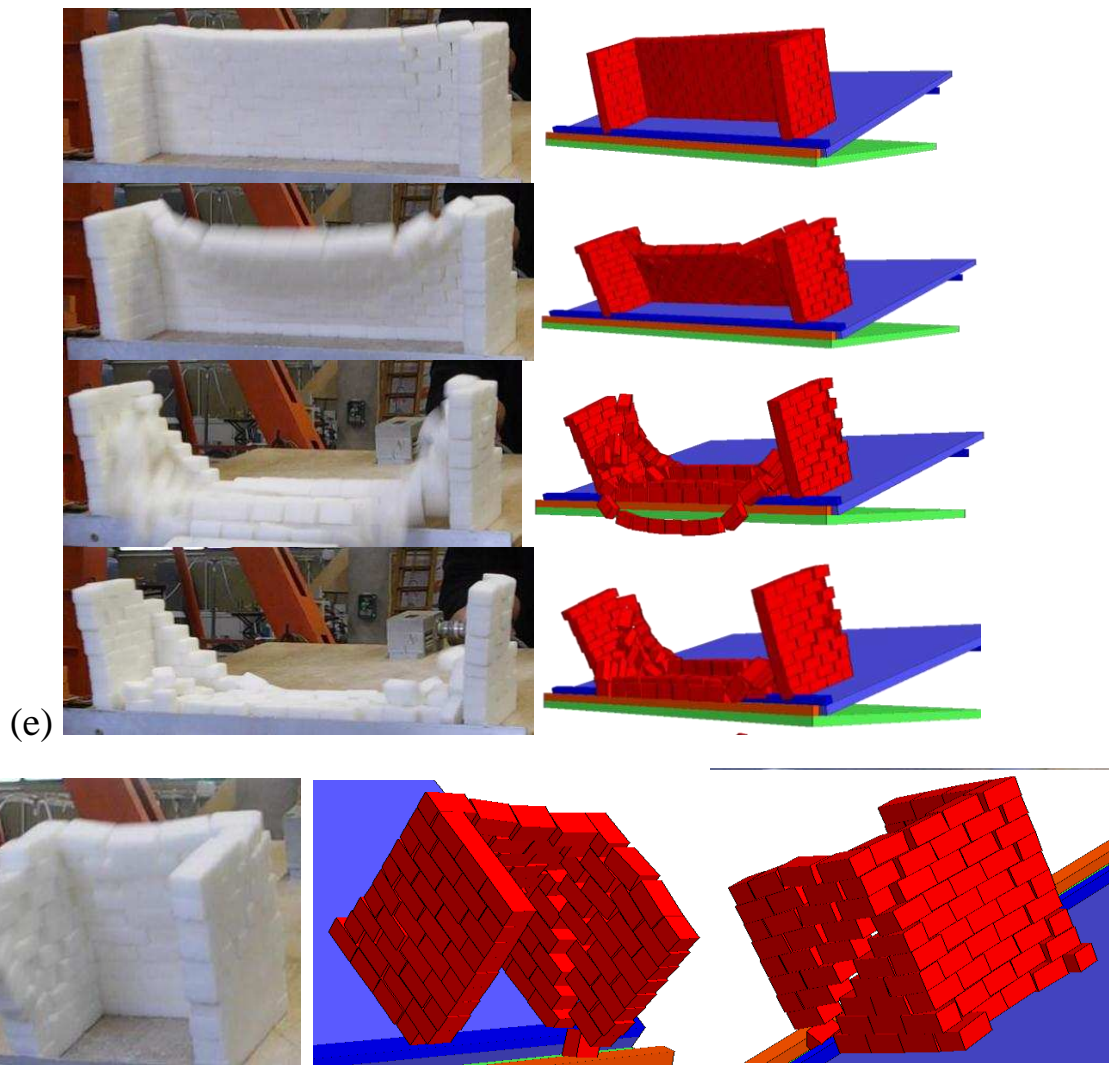


**Figure 9.** Comparison of the collapse mechanism in the experimental test and numerical simulation: a)  $L/H = 3.2$ ; b)  $L/H = 2.768$ ; c)  $L/H = 2.336$ ; d)  $L/H = 1$ ; e)  $L/H = 2.768$ ; f)  $L/H = 1$ .

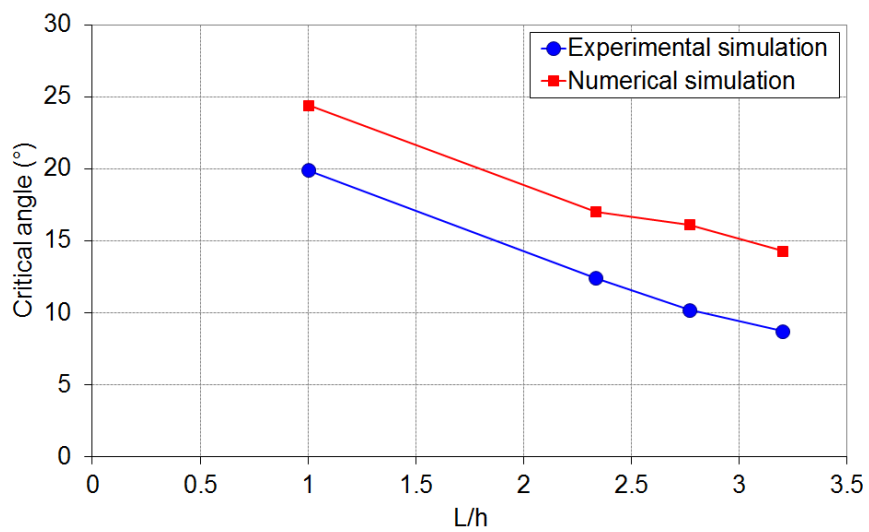


**Figure 10.** Influence of the  $L/H$  ratio on the critical angle: experimental versus numerical simulations

#### 4.2 Harmonic seismic loading– Scaled models 1/10

A series of experimental tests carried out to assess the “box action” effect of a rectangular masonry structure constructed with dry joints and without a roof was subjected to harmonic seismic loading. Each wall was 265 mm in length and made up of ten courses of stretcher-bonded blockwork. In total, the structure was made of 260 masonry blocks. A vibrating table able to sustain a harmonic load with constant amplitude and varied frequency was constructed in the laboratory (**Figure 11**). The vibrating table was square and measured 280 mm × 280 mm, was made of wood and anchored on a rigid metal plate. The harmonic load was applied using a hydraulic jack. The load applied was defined as a function of the amplitude  $A$  and the angular frequency  $\omega$ , using the sinusoidal function:

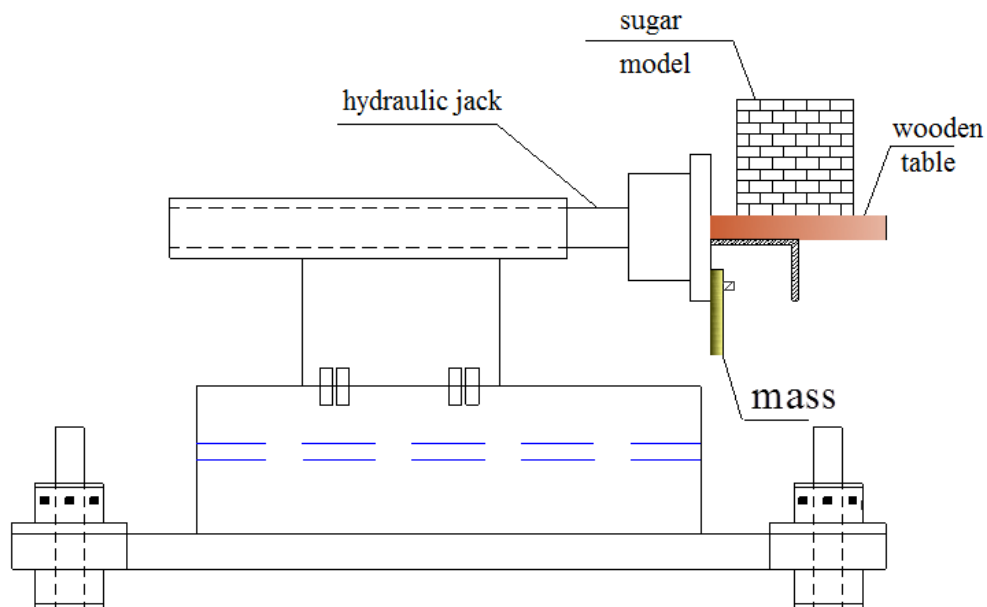
$$y(t)=A \sin(\omega t), \quad (10)$$

where  $y$  is the displacement of the vibrating table,  $A$  is the amplitude of the vibrating table and  $\omega$  is the angular frequency, which was calculated by:

$$\omega = 2 \times \pi \times f \quad (11)$$

Also, the maximum accelerations were calculated by:

$$A_{\max} = -\omega^2 \times A \quad (12)$$



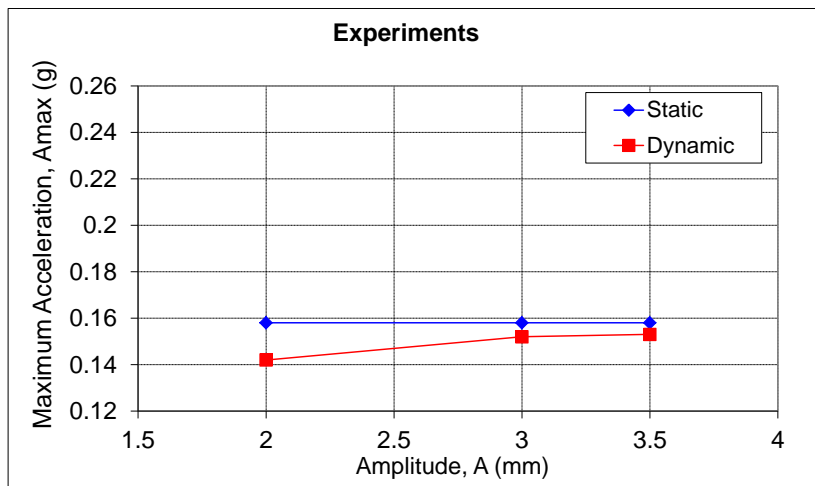
(a)



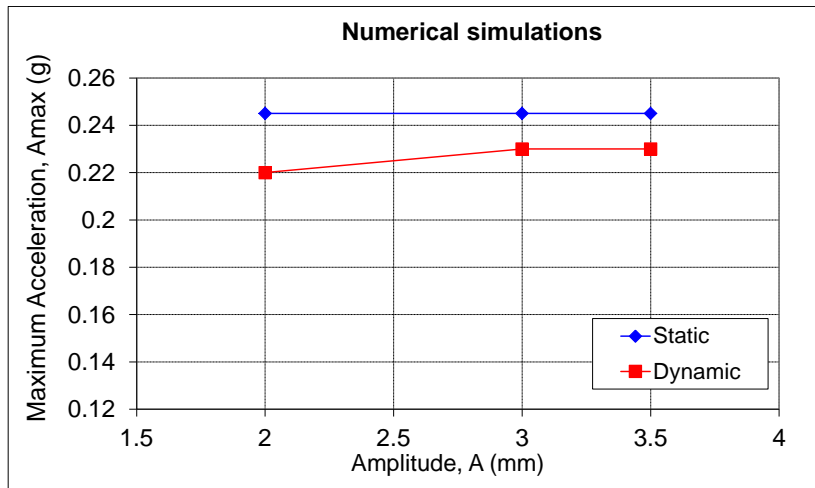
(b)

**Figure 11.** Experimental test set-up

The analysis of the results showed that the predominant failure occurs in the main walls of the structure due to bending. However, excessive damage of the main wall led to cracking and even in some cases partial collapse of the secondary walls. The local failure modes observed from the experimental study are shown in **Figure 13**. Numerical models were developed to represent the dimensions of the walls and the types of loading tested in the experiments. For the development of the numerical model, the material properties for the blocks and joints remained the same as those used in the section 4.1. **Figure 12** compares the experimental and numerical results. **Figure 12** shows that the experimental and numerical results are dissimilar because of the scale effects and the highly heterogeneous behaviour of the masonry blocks made of sugar. **Figure 13** compares the experimental and the numerical model failure patterns; as can be seen, the DEM is able to capture the experimental modes of failure with acceptable accuracy.

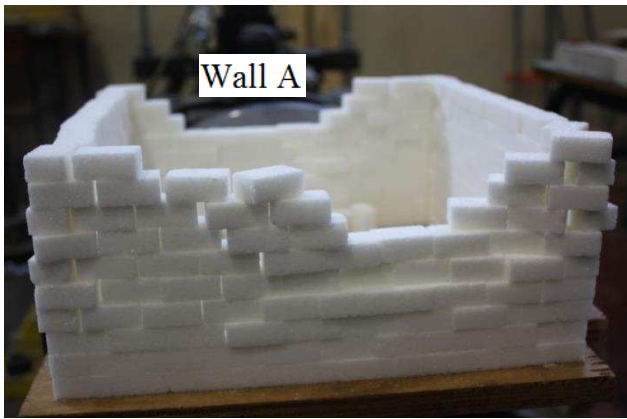


(a)

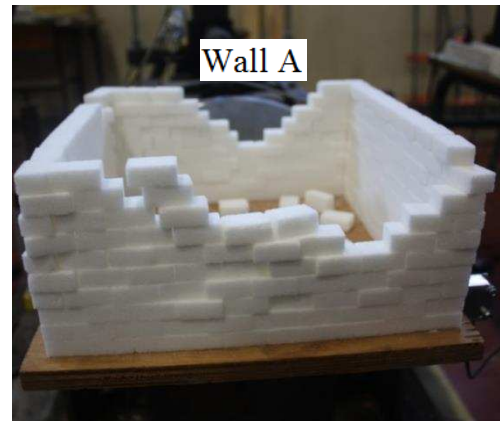


(b)

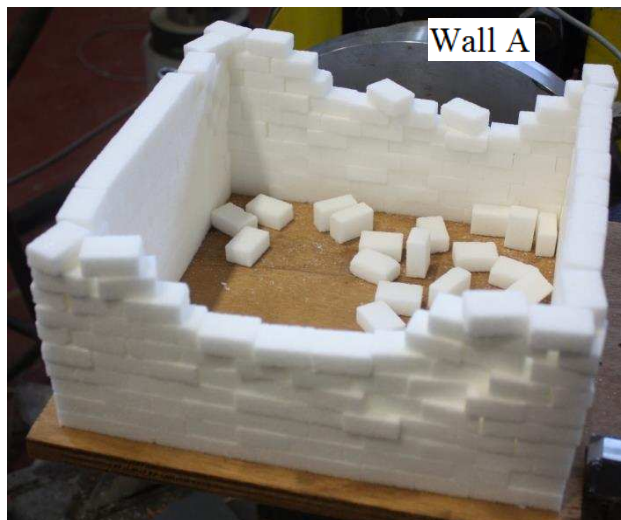
**Figure 12.** Maximum acceleration versus amplitude obtained from: a) experiments; b) numerical simulations



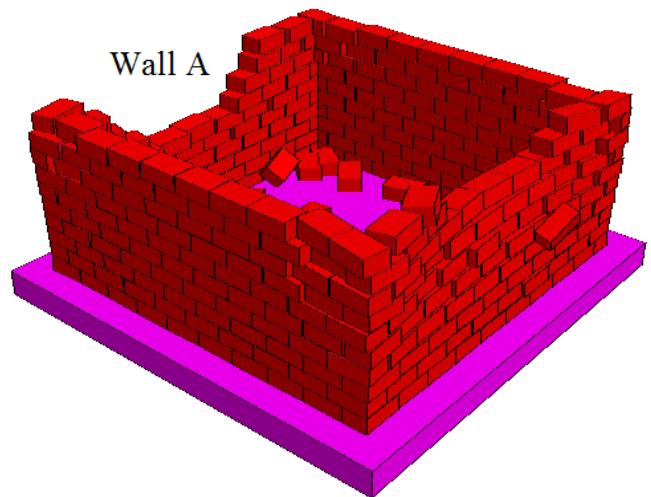
(a) Amplitude 2 mm



(b) Amplitude 3.5 mm



(c) Amplitude 3 mm



(d) Amplitude 3 mm

**Figure 13.** Failure modes for the rectangular masonry structure

#### 4.3 Quasi-static loading – Model scale 1/5

Out-of-plane failure of historical masonry is often a result of equilibrium loss rather than high stress levels. Recurrent mechanisms have been observed in past earthquakes and classifications and possible analytical descriptions proposed by D'Ayala (2003), who introduced a mechanical model based on limit analysis and macro-elements, assuming dry block masonry connected together by pure friction and cohesion. Masonry buildings were composed of three-dimensional assemblies of walls. The collapse mechanisms of the wall assemblies were analysed and ranked depending on the type of damage caused and size of the structure involved. Later, 42 tests were carried out by Restrepo-Velez (2010) in the laboratory of the University of Pavia's Department of Structural Mechanics. Several configurations were built and tested and the out-of-plane collapse mechanisms proposed by D'Ayala (2003) were reproduced (**Figure 14** Mechanisms A–G). The study of Restrepo-Velez (2010) reports the design, the execution and the results of a series of static tests performed on numerous configurations on 1:5 scale dry-stone masonry wall specimens. The suitability of the discrete element method was tested to predict the out-of-plane behaviour of these experimental tests.

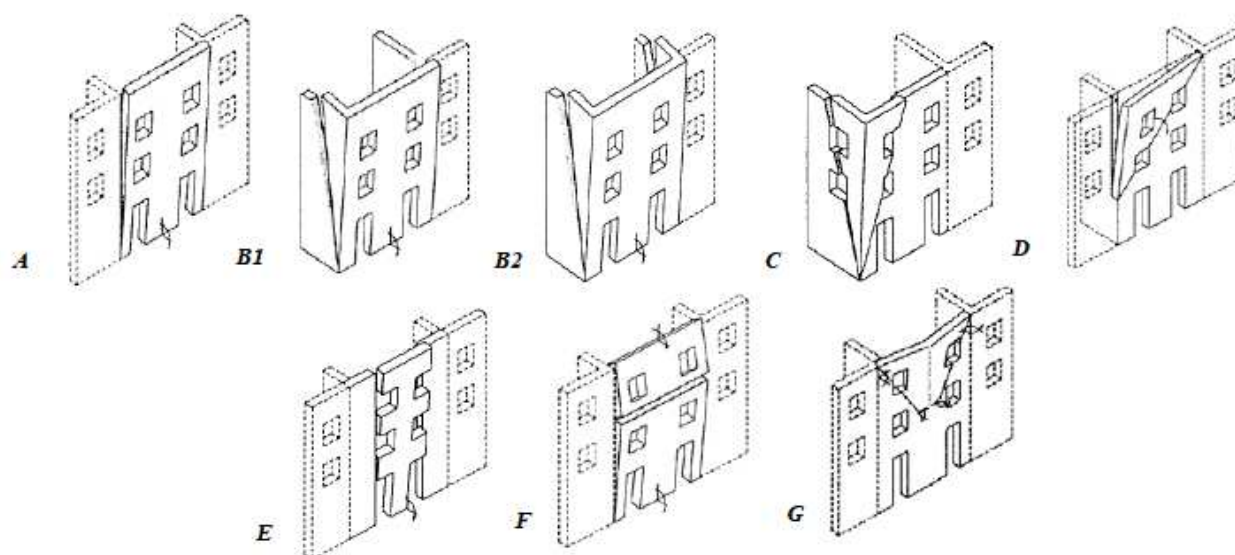


**Figure 14.** A summary of the potential types of failure mechanism observed in masonry structures subjected to out-of-plane loading (D'Ayala, 2003)

The experimental tests were 1:5-scale models and constructed with different geometry masonry walls which were connected with perpendicular partition walls and tested by Restrepo-Velez et al. (2010, 2014). The length-to-height (L/H) ratio of the walls varied (Table 2) and the different modes of failure were investigated. Typical dimensions of the masonry wall constructions tested in the laboratory are shown in **Figure 15**. All walls were made of dry-stone masonry blocks with dimensions equal to 280 mm × 800 mm × 400 mm. Also, the masonry unit weighed 2,680 kg/m<sup>3</sup>. Initially, the model was brought into equilibrium under its self-weight. Then the base of the structure was raised incrementally (every 0.045 degrees) using a tilting table up to the point where collapse occurred. For every experiment, the tilting angle (or the critical angle) and the mode of failure just before the time of the collapse of the structure were recorded. To determine the coefficient of

friction between the masonry blocks, small-scale experimental tests, similar to those reported by Restrepo-Velez (2010), were undertaken. From the analysis of the results it was found that the friction angle varies from 0.67 to 0.77. For the development of the computational model, the friction coefficient of the joint was assumed equal to 0.67, while the cohesive strength, tensile strength and the dilatancy angle of the zero-thickness interfaces were zero. Normal and shear stiffness values were taken low to represent the dry-joint test without significant pre-compression with the same values used in section 4.1. Rigid blocks were specified.

**Table 2.** Summary of experimental tests and variation of the length-to-height ratio of the main wall in the masonry structure

Test No.	Length to height of the main wall (L/H)	Number of blocks spanning the main wall
S1	1.50	11
S2	1.50	11
S3	1.50	11
S5	1.09	8
S6	1.77	13

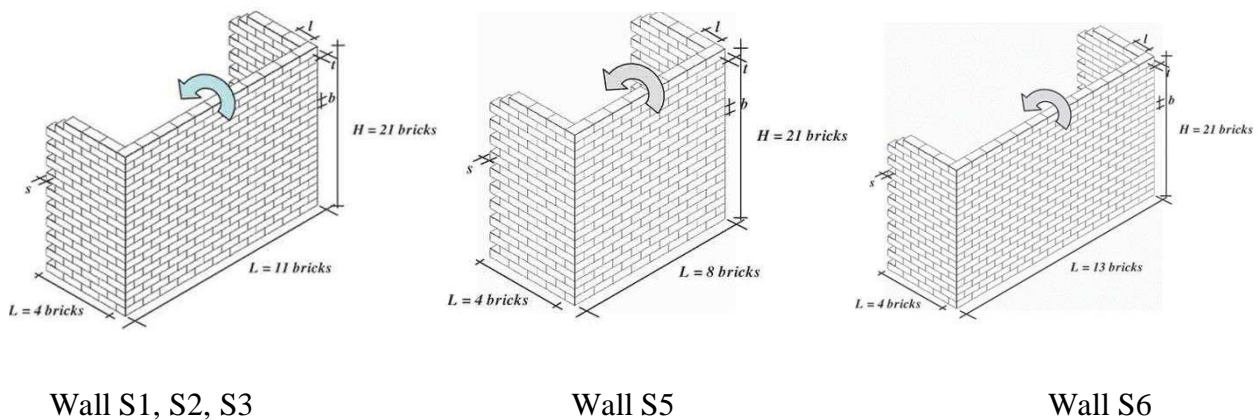
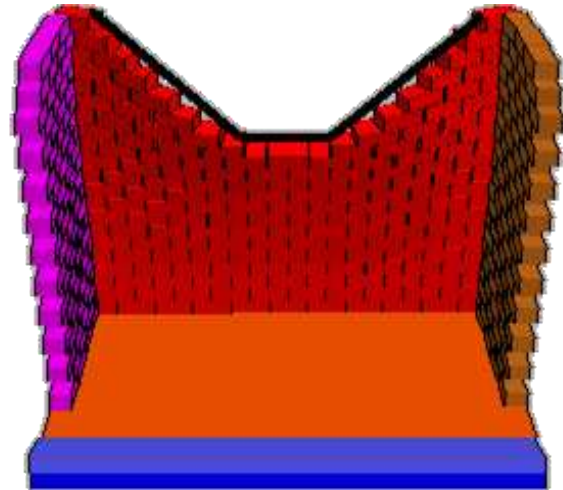
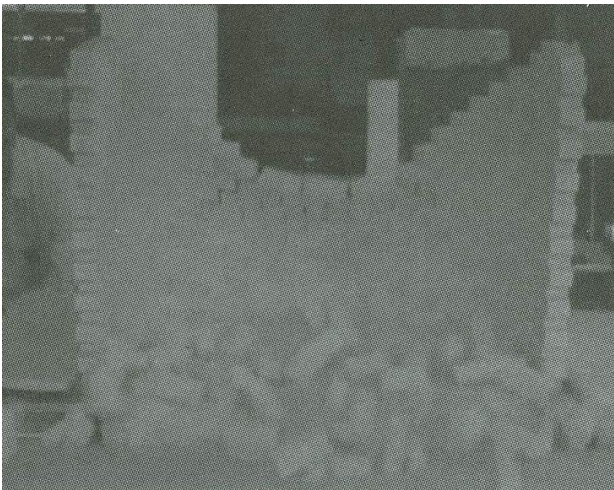


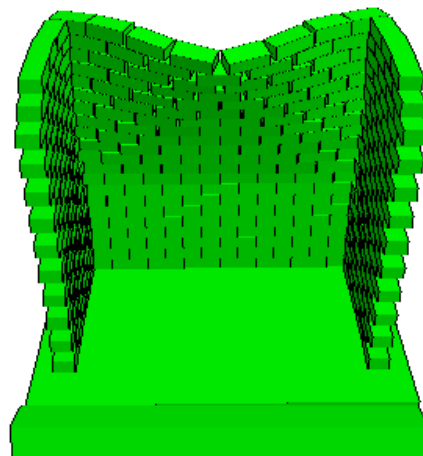
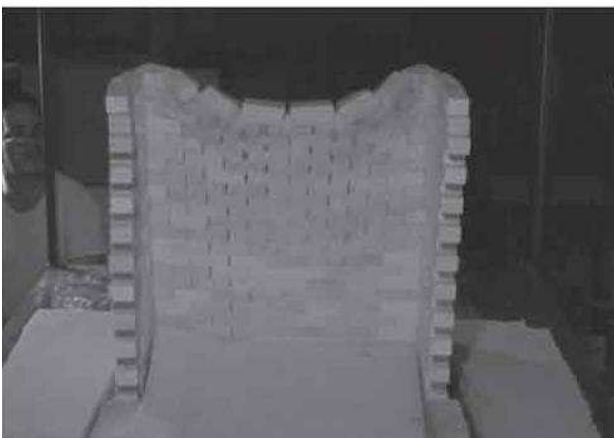
**Figure 15.** Geometric configuration of the different masonry wall constructions tested in the laboratory by Restrepo-Velez et al. (2010)

Firstly, the mechanism G was analysed by studying the mechanical behaviour of a main wall assembled with two partition walls. Three configurations were studied to analyse the influence of length/height (L/H) fraction of the main wall. For the L/H fraction equal to 1.5 (with N=11 bricks on the length wall), three tests were carried out with the same geometry (wall S1, S2, S3). For the two other L/H configurations equal to 1.09 (wall S5, with N=8 bricks on the length wall) and L/H equal to 1.77 (wall S6, with N=13 bricks on the length wall), only one test was conducted for each configuration. **Figure 16** compares the failure modes observed in the experimental study with those predicted using the numerical models developed for the different cases studied. In **Figure 16**, it can be seen that the computational model developed is capable of predicting the

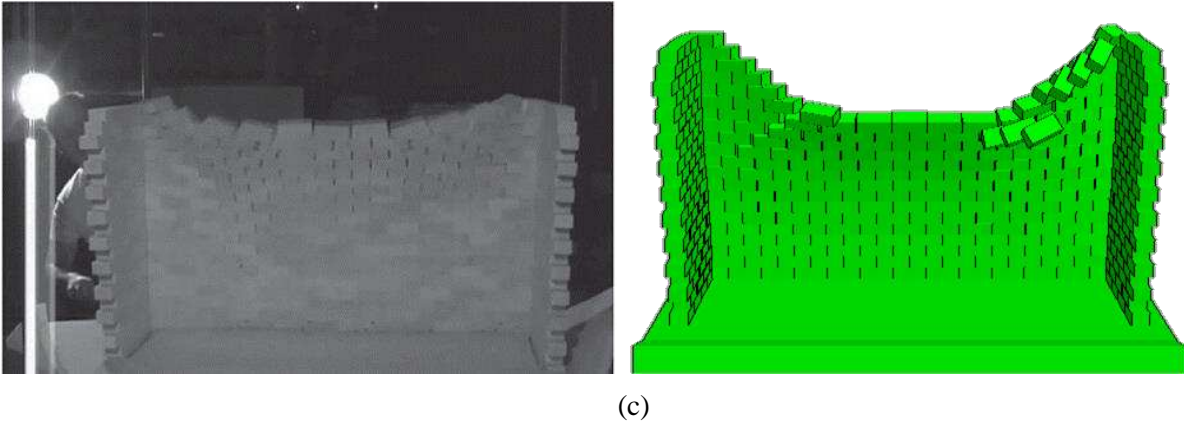
development of the experimental failure mode with sufficient accuracy. Both the experimental and numerical results show that the failure mechanism is characterized by a trapezoidal central portion with two tear lines: vertical and diagonal cracking. This is failure mode G (**Figure 14**) as per the classification derived from D'Ayala (2003). In the wall panels, vertical cracks initiated due to pure frictional resistance between adjacent masonry unit blocks while shear cracks developed due to the development of shear stresses and excessive rotation due to out-of-plane bending moments. The development of such failure modes was reported in Casapulla (2008), where an analytical method for determining the multiplier is explicitly discussed. This study developed a new simplified procedure to evaluate upper and lower thresholds for the possible collapse load factor for in-plane and out-of-plane loaded block masonry structures with frictional resistance, by means of limit state analysis. A particular class of mechanisms characterized by out-of-plane torsion-shear interactions on frictional interfaces was analysed. Bypassing a detailed discrete element analysis, it was assumed herein that the general failures involved a number of cracks which separate the structures into a few macro-blocks and that all the possible relative motions among micro-blocks are concentrated along the cracks.



(a)



(b)



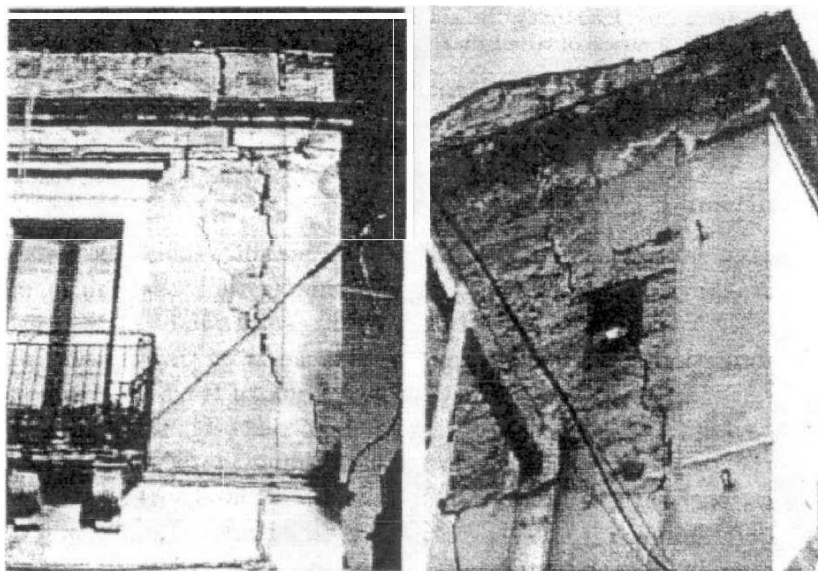
**Figure 16.** Comparison of the failure modes observed experimentally (Restrepo-Velez et al. 2010) versus numerical simulation predictions obtained from the discrete element method for the different cases studied: a) Wall S1; b) Wall S5; c) Wall S6.

Table 3 compares the experimental ( $\lambda_{exp}$ ) and numerical results derived by the DEM ( $\lambda_{DEM}$ ) and the analytical results (match  $\lambda_1, \lambda_2$  alternately) as proposed by D'Ayala (2003) and (Casapulla, 2008) for failure mode G. Overall, the numerical results derived by the DEM and the analytical results as per Casapulla (2008) demonstrate a decreasing trend of  $\lambda$  as the L/H ratio increases. However, the analytical method proposed by D'Ayala (2003), which is based on the effect of the arches, cannot reproduce this trend. The values obtained by D'Ayala (2003) have large deviations from the experimental results since torsional friction along the sloped crack line is not taken into account. The analytical method proposed by Casapulla (2008) which takes into account the torsional and shear effects, provides a good agreement with the numerical results for the collapse coefficient in the case of the upper bounds solutions ( $\lambda_2$  upper). However, in comparison with the lower bounds solutions ( $\lambda_2$  lower) the analytical approach is conservative and underestimates the results obtained from the experiment.

**Table 3.**  $\lambda$  for the failure mode G

Test	L/H	$\lambda_{exp}$	DEM		[D'Ayala, 2003]		[Cassapulla, 2008]			
			$\lambda_{DEM}$	Difference (%)	$\lambda_1$	Difference (%)	$\lambda_2$ (upper)	Difference (%)	$\lambda_2$ (lower)	Difference (%)
S1	1.500	0.254	0.262	<b>-3.15</b>	0.222	<b>12.60</b>	0.266	<b>-4.72</b>	0.186	<b>26.77</b>
S2	1.500	0.226	0.262	<b>-15.93</b>	0.222	<b>1.77</b>	0.266	<b>-17.70</b>	0.186	<b>17.70</b>
S3	1.500	0.244	0.262	<b>-7.38</b>	0.147	<b>39.75</b>	0.266	<b>-9.02</b>	0.186	<b>23.77</b>
S5	1.090	0.349	0.327	<b>6.30</b>	0.187	<b>46.42</b>	0.346	<b>0.86</b>	0.247	<b>29.23</b>
S6	1.770	0.208	0.218	<b>-4.81</b>	0.279	<b>-34.13</b>	0.230	<b>-10.58</b>	0.160	<b>23.08</b>

Investigations into the suitability of the model to capture mechanisms A and B2, which often recur in the investigation of historical buildings after an earthquake (**Figure 17**), were undertaken. The mechanical behaviour of such structures depends on the quality and strength of the connections between elements of the structure including partition walls, internal load-bearing partitions, floors and roof structures. The type A mechanism corresponds to the overturning of the façade wall when there is poor or no connection with the orthogonal walls (**Figure 17a**). The type B2 mechanism occurs instead of type A mechanism when the level of connection is sufficient to involve, beyond the main wall, one or both partition walls in the overturning, due to a sufficient length of overlapping between elements common to both walls. These mechanisms are developed by the occurrence of a diagonal crack along the partition walls and a horizontal hinge on the façade (**Figure 17b**). To reproduce mechanism A or B2, models representing the tests S7, S8, S9, S10 (with the L/H variable) were created (Restrepo-Velez, 2010). The analysis of the results showed that the failure mode generated from these tests is a mixture of both mechanisms A and B2. Mechanism B2 was produced only by tests S22 and S42 due to the presence of singularities in the transverse walls. Table 4 shows a comparison between the values obtained in the experimental tests ( $\lambda_{exp}$ ) and the numerical results of DEM ( $\lambda_{DEM}$ ) and the analytical results previously reported in the literature (D'Ayala, 2003; Vaculik, 2010). Comparisons between the experimental and numerical failure modes are shown in **Figure 18** to **Figure 21**. These tests showed that discrete element modelling is a viable approach to assess structural integrity and predict the failure mode of such masonry structures.



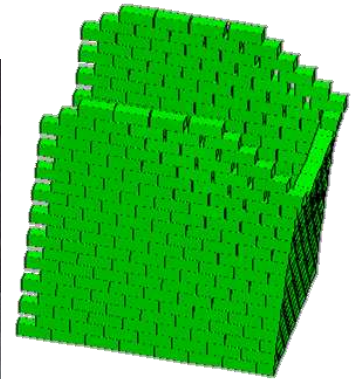
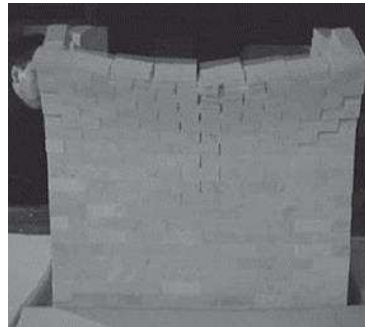
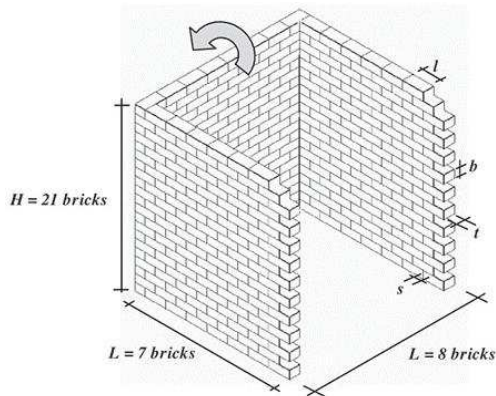
(a) - Mechanism A

(b) – Mechanism B2

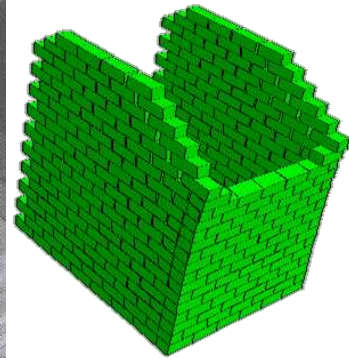
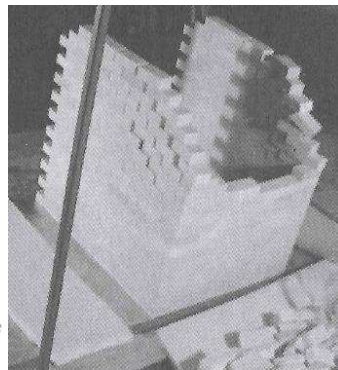
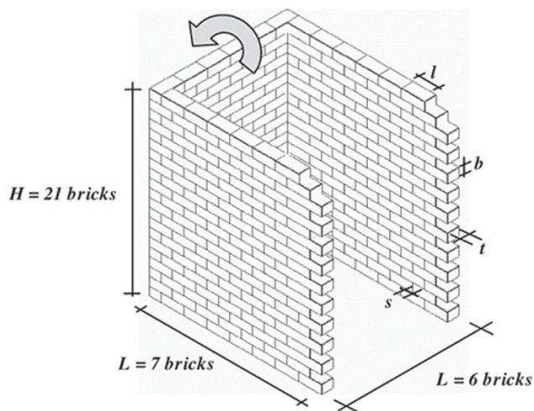
**Figure 17.** Excessive damage observed in traditional masonry building resulting from the Carlentini earthquake, Sicily 1990 (De Felice, 2001) corresponds to mechanism A and mechanism B2 (to be read in conjunction with **Figure 14**)

**Table 4.**  $\lambda$  for the failure mode A-B2

Test	L/H	$\lambda_{exp}$	DEM		[D'Ayala, 2003]		[Vaculik, 2010]	
			$\lambda_{DEM}$	Difference (%)	$\lambda_1$	Difference (%)	$\lambda_2$	Difference (%)
S7	1.088	0.291	0.287	<b>1.37</b>	0.438	<b>-50.52</b>	0.273	<b>6.19</b>
S8	0.816	0.362	0.326	<b>9.94</b>	0.506	<b>-39.78</b>	0.352	<b>2.76</b>
S9	0.816	0.352	0.326	<b>7.39</b>	0.545	<b>-54.83</b>	0.352	<b>0.00</b>
S10	1.633	0.213	0.221	<b>-3.76</b>	0.356	<b>-67.14</b>	0.190	<b>10.80</b>
S22	x	0.197	0.186	<b>5.58</b>	x	<b>x</b>	x	<b>x</b>
S42	x	0.236	0.196	<b>16.95</b>	x	<b>x</b>	x	<b>x</b>



(a) Test S7



(b) Test S8-S9

**Figure 18.** Observed experimental failure mechanisms (Restrepo-Velez et al. 2010) versus those predicted by the discrete element method for the masonry construction S7, S8, S9 (A-B2 mechanism)

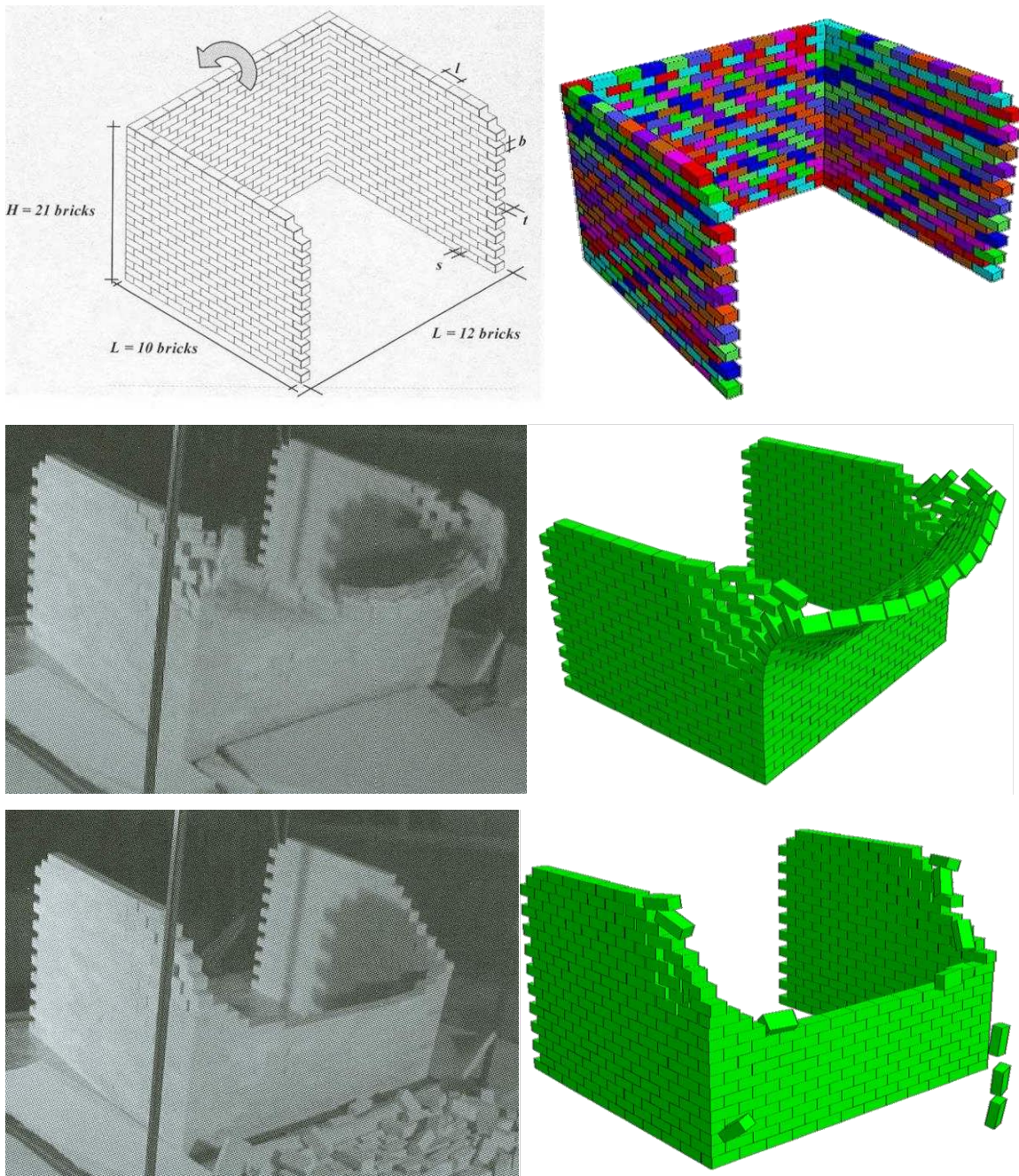


**Figure 19.** Observed experimental failure mechanisms (Restrepo-Velez et al. 2010) versus those predicted by the discrete element method for the masonry construction S10 (A- B2 mechanism)

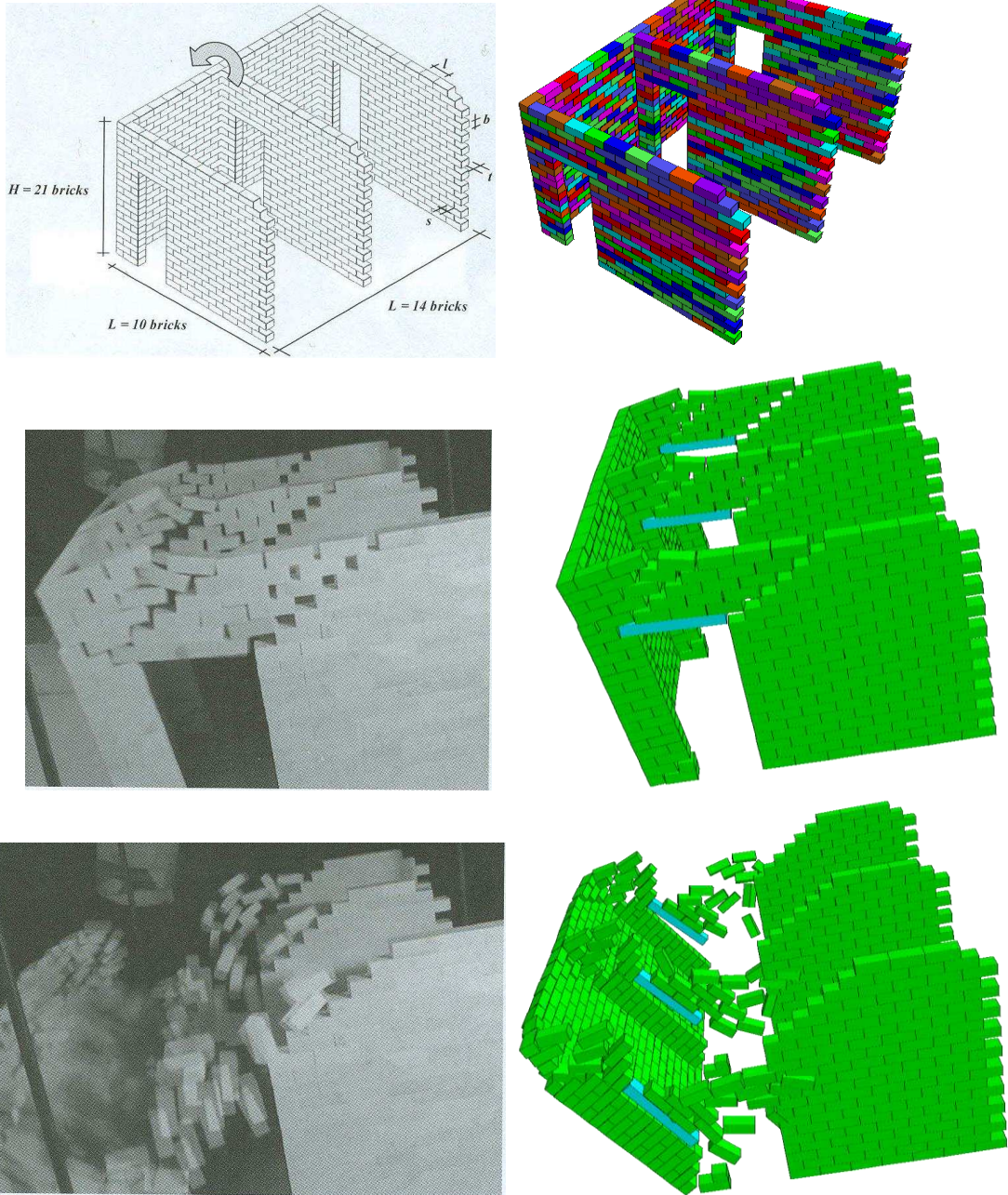


**Figure 20.** Observed experimental failure mechanisms (Restrepo-Velez et al. 2010) versus those predicted by the discrete element method for the masonry construction S22 (B2 mechanism).

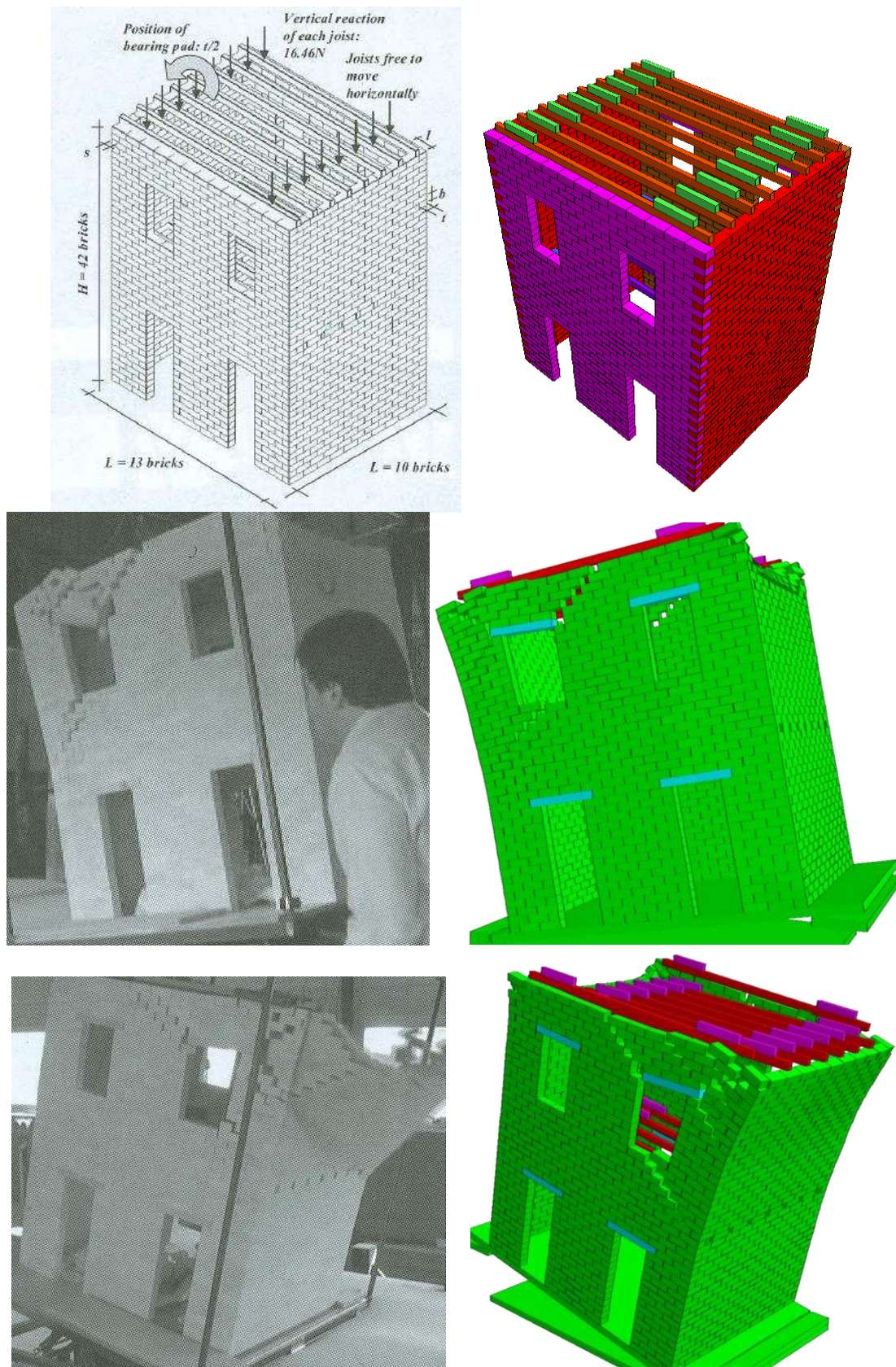


**Figure 21.** Observed experimental failure mechanisms (Restrepo-Velez et al. 2010) versus those predicted by the discrete element method for the masonry construction S42 (B2 mechanism).

In section 4, **Figures 10** and **12** show fairly poor agreement. Firstly, for the 1/10 scale (sections 4.1 and 4.2), we found that the numerical results (critical angle) overestimated the experimental results, the gap is mainly provided by the scale effects. In the example with small specimens (scale 1/10), the nature of the block-to-block interface is more complex than the Coulomb friction model used in this study. It can often occur that even the most sophisticated friction model does not fully reflect the friction characteristics generated experimentally due to the influence of certain random factors (e.g. variations of normal pressure force or inhomogeneous asperity of contacting surfaces, etc.). Especially when the specimen's dimension is small, as in our case, the influence of inhomogeneous asperity of contacting surfaces and of the other random factors could be amplified. This point causes the difference between the numerical and experimental results for the small-scale test in sections 4.1 and 4.2.

In fact, when a full-scale structure is considered, as in section 4.3, the numerical model gave very good results when compared with the experimental results. To resolve this problem, a more sophisticated constitutive law should be used to represent the frictional resistance between interfaces. The development of this model is not within the scope of this research. However, this is suggested as future research at the end of the conclusion section.

## 5. Conclusions

In this paper, the suitability of the DEM to simulate the in-plane and out-of-plane behaviour of masonry walls constructed with dry joints has been investigated. The assessment consisted of a comparison of the results from full-scale laboratory tests and those from the scaled model tests (model scale 1/10 and model scale 1/5) versus the behaviour predicted using the three-dimensional DE modelling software, 3DEC. A key feature of the DE method is the important role that discontinuities, i.e. joints, play in the mechanics of the masonry. Within 3DEC, the bricks were modelled as continuum elements while the joints were modelled by line-interface elements represented by the Coulomb friction law. A significant feature of the research was the collection of experimentally verified material parameters that could reliably be used by other researchers and engineers worldwide to solve engineering challenges.

Analysing these results, it was found that the DEM is a viable approach for the prediction of the ultimate load and failure mode analysis of masonry walls constructed with dry joints subjected to in-plane and out-of-plane loading. Also, the possibility of frequent changes in the connectivity and the type of contact as well as marked non-linearity induced by the inability of the masonry joints to withstand tension, makes the DEM a suitable approach for solving problems involving discontinuities, as is the case with masonry constructed with dry joints. The dimensions of the blocks and the geometrical configuration of such structures greatly affect the failure load and failure mechanism. Table 5 summarizes the capabilities and limitations of the DEM for modelling the in-plane and out-of-plane behaviour of masonry constructed with dry mortar joints. Future studies will use advanced constitutive laws of friction as a function of velocity to assess the influence of Stribeck friction (Wojewoda et al. 2008) on the out-of-plane behaviour of dry-joint masonry structures.

**Table 5.** Capabilities and limitations of the DEM for modelling the in-plane and out-of-plane behaviour of masonry constructed with dry mortar joints.

<b>Capabilities</b>	<b>Limitations</b>
<ul style="list-style-type: none"> <li>• Large displacements and rotations of the units are allowed.</li> <li>• Ability to mesh the blocks independently, without the need to match nodal points.</li> <li>• Same algorithm for static and dynamic analysis.</li> <li>• Capable of modelling post-peak behaviour until collapse.</li> <li>• Overlap of units is restricted and dilation effects could be included.</li> </ul>	<ul style="list-style-type: none"> <li>• Computationally expensive when dealing with large structures.</li> <li>• Scale effects could lead to inaccurate results.</li> <li>• Incapable of capturing behaviour of structures with highly heterogeneous interface elements.</li> </ul>

## References

- Bui, T.T. Bui, Q.B. Limam A. Morel J.-C. (2015). Modeling rammed earth wall using discrete element method. *Continuum Mechanics and Thermodynamics*, 28(1-2), pp.523–538.
- Bui, T.T. and Limam, A. (2012). Masonry Walls under Membrane or Bending Loading Cases: Experiments and Discrete Element Analysis. In *The Eleventh International Conference on Computational Structures Technology*. p. Paper 119.
- Bui, T.T. and Limam, A. (2014). Out-of-plane behaviour of hollow concrete block masonry walls unstrengthened and strengthened with CFRP composite. *Composites Part B: Engineering*, 67, pp.527–542.
- Bui, T.T., Limam, A. and Bui, Q.B. (2014). Characterisation of vibration and damage in masonry structures: experimental and numerical analysis. *European Journal of Environmental and Civil Engineering*, 18(10), pp.1118–1129.
- Casapulla, C. (2008). Lower and upper bounds in closed form for out-of-plane strength of masonry structures with frictional resistances. *Proc. of the 6th Int. Conf. on Structural Analysis of Historical Constructions*, 2, pp.1191–1198.
- Casapulla C, Cascini L, Portioli F, Landolfo R (2014). 3D macro and micro-block models for limit analysis of out-of-plane loaded masonry walls with non-associative Coulomb friction. *Meccanica* 49(7):1653-78.
- Chaimoon, K. and Attard, M.M. (2007). Modeling of unreinforced masonry walls under shear and compression. *Engineering Structures*, 29(9), pp.2056–2068.

- Claxton, M., Walker, P. and McCombie, P. (2007). Plane strain numerical model for drystone retaining walls. *Proceedings of the ICE - Geotechnical Engineering*, 160(2), pp.97–103.
- Cundall, P.A. and Hart, R.D. (1992). Numerical Modelling of Discontinua. *Engineering Computations*, 9(2), pp.101–113.
- D’Ayala, D. and Speranza, E. (2003). Definition of collapse mechanisms and seismic vulnerability of masonry structures. *Earthquake Spectra*, 19(3), pp.479-509.
- DeJong, M.J. Seismic assessment strategies for masonry structures. Ph.D. dissertation. Massachusetts Institute of Technology, Cambridge, UK. 2009
- Felice, G.D. and Giannini, R. (2001). Out-of-Plane Seismic Resistance of Masonry Walls. *Journal of Earthquake Engineering*, 5(2), pp.253–271.
- Giamundo V., Sarhosis V., Lignola G.P., Sheng Y., Manfredi G. (2014). Evaluation of different computational modelling strategies for the analysis of low strength masonry structures. *Engineering Structures*, 73, pp.160–169.
- Heyman, J. (1998). *Structural Analysis: A Historical Approach*. Cambridge University Press.
- ITASCA, 3DEC (2002) – Three Dimensional Distinct Element Code, Version 4.0, Itasca, Minneapolis.
- Lagomarsino, S. and Resemini, S. (2009). The Assessment of Damage Limitation State in the Seismic Analysis of Monumental Buildings. *Earthquake Spectra*, 25(2), pp.323–346.
- Lemos, J.V. (2004). Modelling stone masonry dynamics with 3DEC. In: H. Konietzky (ed.). *Numerical modelling of discrete materials in geotechnical engineering, civil engineering and earth sciences*. Taylor and Francis Group, London, UK, pp.7-13.
- Lourenço B.P.; Oliveira V.D.; Roca P.; and Orduña A. (2005). Dry Joint Stone Masonry Walls Subjected to In-Plane Combined Loading. *Journal of Structural Engineering*, 131(11), pp.1665–1673.
- Lourenco, P.B. (2000). Aspects Related to the Out-of-Plane Numerical Modelling of Masonry. *Masonry International Journal*, 14, pp.4–31.
- Lourenco, P.B. (1996). Computational strategies for masonry structures. Dissertation. TU Delft, Delft University of Technology, Netherlands
- Lourenço, P.B. (2002). Computations on historic masonry structures. *Progress in Structural Engineering and Materials*, 4(3), pp.301–319.
- Lourenço, P. and Rots, J. (1997). Multisurface Interface Model for Analysis of Masonry Structures. *Journal of Engineering Mechanics*, 123(7), pp.660–668.
- Macchi, G. (1992). Structural diagnosis and rehabilitation of historical buildings. *Cuadernos Intemac*, 7.
- Mohebkah, A., Tasnimi, A.A. and Moghadam, H.A. (2008). Nonlinear analysis of masonry-infilled steel frames with openings using discrete element method. *Journal of Constructional Steel Research*, 64(12), pp.1463–1472.

- Munjiza, A. (2004). *The Combined Finite-Discrete Element Method*. Wiley.
- Oliveira, D.V. (2003). *Experimental and numerical analysis of blocky masonry structures under cyclic loading*. Ph.D thesis, University of Minho, Minho, Portugal.
- Otter, J.R.H., Cassell, A.C. and Hobbs, R.E. (1966). Dynamic relaxation. *Proceedings of the Institution of Civil Engineers* 35, pp.633–665.
- Page, A.W. (1978). Finite element model for masonry. *Journal of the Structural Division, ASCE*, 104(8), pp.1267–1285.
- Papantonopoulos, C. Psycharis I.N., Papastamatiou, D.Y. Lemos, J.V., Mouzakis H. P. (2002). Numerical prediction of the earthquake response of classical columns using the distinct element method. *Earthquake Engineering & Structural Dynamics*, 31(9), pp.1699–1717.
- Psycharis I. N., Lemos J. V., Papastamatiou D. Y., Zambas C. and Papantonopoulos C. (2003). Numerical study of the seismic behaviour of a part of the Parthenon Pronaos. *Earthquake Engineering & Structural Dynamics*, 32(13), pp.2063–2084.
- Restrepo-Vélez, L.F., Magenes, G. and Griffith, M.C. (2014). Dry Stone Masonry Walls in Bending—Part I: Static Tests. *International Journal of Architectural Heritage*, 8(1), pp.1–28.
- Restrepo-Vélez, L.F., Magenes, G. (2010). *Static Tests on Dry Stone Masonry and Evaluation of Static Collapse Multipliers*, Research Report ROSE, Iuss Press, Pavia, Italy.
- Roberti, G.M. (2001). Discrete element analysis on the Sardinian “Nuraghe”. In: P.B. Lourenço, P. Roca (eds.), *Historical Constructions*. Guimarães, 7-9 November, University of Minho, Portugal, pp.719-727.
- Roberti, G.M. and Calvetti, F. (1998). Distinct element analysis of stone arches. In: Sinopolo (ed.), *Proceedings of the Second International Conference on Arch Bridges*. Italy, Venice, pp.181-186.
- Rots. (1997). *Structural Masonry: An Experimental/ Numerical Basis for Practical Design Rules* (CUR Report 171). CRC Press.
- Sarhosis, V., Oliveira, D.V., Lemos J.V., Lourenco P.B. (2014). The effect of skew angle on the mechanical behaviour of masonry arches. *Mechanics Research Communications*, 61, pp.53–59.
- Sarhosis, V., Garrity, S.W. and Sheng, Y. (2015). Influence of brick–mortar interface on the mechanical behaviour of low bond strength masonry brickwork lintels. *Engineering Structures*, 88, pp.1–11.
- Sarhosis, V. and Sheng, Y. (2014). Identification of material parameters for low bond strength masonry. *Engineering Structures*, 60, pp.100–110.
- Sarhosis, V., Tsavdaridis, K.D. and Giannopoulos, I. (2014). Discrete Element Modelling of Masonry Infilled Steel Frames with Multiple Window Openings Subjected to Lateral Load Variations. *The Open Construction and Building Technology Journal*, 8(1), pp.93–103.
- Sarhosis V, Asteris P, Wang T, Hu W, Han Y. (2016). On the stability of colonnade structural systems under static and dynamic loading conditions. *Bulletin of Earthquake Engineering*, 14(4), 1131-1152.

Tóth, A.R., Orbán, Z. and Bagi, K. (2009). Discrete element analysis of a stone masonry arch. *Mechanics Research Communications*, 36(4), pp.469–480.

Vaculik, J., Griffith, M. and Magenes, G. (2010). Collapse load predictions for masonry walls in bending. In *Proceedings, 8th International Masonry Conference, Dresden, Germany*.

Wojewoda J, Stefański A, Wiercigroch M, Kapitaniak T (2008) Hysteretic effects of dry friction: modelling and experimental studies. *Phil. Trans. R. Soc. A* 366: 747-765